



저작자표시-비영리-변경금지 2.0 대한민국

이용자는 아래의 조건을 따르는 경우에 한하여 자유롭게

- 이 저작물을 복제, 배포, 전송, 전시, 공연 및 방송할 수 있습니다.

다음과 같은 조건을 따라야 합니다:



저작자표시. 귀하는 원저작자를 표시하여야 합니다.



비영리. 귀하는 이 저작물을 영리 목적으로 이용할 수 없습니다.



변경금지. 귀하는 이 저작물을 개작, 변형 또는 가공할 수 없습니다.

- 귀하는, 이 저작물의 재이용이나 배포의 경우, 이 저작물에 적용된 이용허락조건을 명확하게 나타내어야 합니다.
- 저작권자로부터 별도의 허가를 받으면 이러한 조건들은 적용되지 않습니다.

저작권법에 따른 이용자의 권리는 위의 내용에 의하여 영향을 받지 않습니다.

이것은 [이용허락규약\(Legal Code\)](#)을 이해하기 쉽게 요약한 것입니다.

[Disclaimer](#)

공학석사학위논문

Micro-Injection Molding of Glass Fiber Reinforced Parts

유리 섬유가 강화된 부품의
미세 사출 성형

2014년 2월

서울대학교 대학원

재료공학부

황 순 형

Micro-Injection Molding of Glass Fiber Reinforced Parts

유리 섬유가 강화된 부품의

미세 사출 성형

지도 교수 윤 재 룬

이 논문을 공학석사 학위논문으로 제출함

2014 년 2월

서울대학교 대학원

재료공학부

황 순 형

황순형의 석사 학위论문을 인준함

2014년 2월

위 원 장 _____ (인)

부위원장 _____ (인)

위 원 _____ (인)

Micro-Injection Molding of Glass Fiber Reinforced Parts

Advisor: Jae Ryoun Youn

by
Soon Hyung Hwang

2014

Department of Materials Science and Engineering

Graduate School

Seoul National University

ABSTRACT

Micro injection molding has recently gained tremendous attention owing to an increased demand for microelectromechanical systems (MEMS) and microsystems which encompass a wide range of industrial and engineering applications. Since the sizes of microinjection molded parts and devices are typically on the order of hundreds of micrometers, its flowability of molten polymer in a mold cavity becomes important to inject the molten polymers successively during the filling and packing stages during the injection molding. Particularly, the rheological properties of the injection molding materials play an important role in the flowability during an injection process due to the fact that the rheological properties are mainly affected by shear rate and temperature which are pragmatic approach to change injection molding conditions. The rheological properties affecting the flowability of molten polymers are extensively characterized by investigating fiber length distribution, volume fraction, and heat transfer of inclusions so as to determine the crucial parameters for the flowability inside micro-sized pitches and channels. Therefore, we firstly fabricated a thin tensile specimen and

investigated the internal structures of the specimen by using Micro-CT to analyze the fiber length distribution of the samples. The data acquired by the Micro-CT was then processed by an image processing to analyze quantitative probability density functions, cumulative functions and probability functions. Also we compared it with several statistical fiber breakage models. From the fiber length distribution results, 3D internal structures of microinjection molded parts were obtained. The results of fiber orientation and flowability were compared with a numerical analysis by using a commercial software tool (MOLDFLOW). Both the experimental and numerical results indicated that long glass fibers, low volume fraction, and low thermal conductivity of inclusions show better flowability. Effective elastic modulus was measured and predicted by combining the theoretical modes.

Keywords: microinjection molding, fiber length distribution, 3D internal structure, composites, numerical analysis

Student Number : 2012-20643

CONTENTS

ASTRACT

List of figures and tables

I. INTRODUCTION

- 1.1. Overview of injection molding
- 1.2. Overview of FLD and Micro-CT
- 1.3. Objective of this work

II. THEORETICAL BACKGROUND

- 2.1. Parameter effects on viscosity
 - 2.1.1. Volume fraction
 - 2.1.2. Fiber Length Distribution (FLD)
 - 2.1.3. Thermal conductivity
- 2.2. Theoretical model
 - 2.2.1. Weibull distribution function
 - 2.2.2. Lognormal distribution function
 - 2.2.3. GEV distribution function
- 2.3. Generalized Newtonian fluid model

2.3.1. Cross-WLF model

III. EXPERIMENTS

3.1. Sample characterization

3.1.1. Materials

3.2. Overview of analysis methods

3.2.1. Incineration

3.2.2. Thermo Gravimetric Analysis (TGA)

3.2.3. Thermo Mechanical Analyzer (TMA)

3.2.4. Scanning Electron Microscope (SEM)

3.2.5. Micro-CT imaging and image processing

3.2.6. Flowability test

3.2.7. Universal testing machine (UTM)

IV. RESULTS AND DISCUSSION

4.1. Anisotropic property of LCP

4.2. Volume fraction and morphological analysis

4.2.1. Incineration

4.2.2. Morphological analysis

4.3. Quantification of fiber length distribution

4.3.1. Image processing

4.3.2. FLD & Theoretical analysis

4.3.3. FLD & 3D structure

4.4. Injection molding & Numerical analysis

4.4.1. Flowability results in spiral channel

4.4.2. Flowability results Analysis in micro-part

4.4.3. Result of Thermo Gravimetric Analysis (TGA)

4.5. Thermal conductivity

4.5.1. Dependence of thermal conductivity coefficient

4.6. Cross WLF model and n coefficient

4.7. Real, Micro-CT, 3D images with line intensity analysis

4.8. Effective elastic modulus

V. CONCLUSION

REFERENCES

KOREAN ABSTRACT

List of figures and tables

Figure 1. Overview of injection molding

Figure 2. Parameters influence on the viscosity

Figure 3. Image of the spiral channel.

Figure 4.1. Incineration result of S1 and S2 with volume fraction of glass fibers and minerals.

Figure 4.2. SEM images of S1 with (a) X50 (b) X100 (c) X150 (d) X200.

Figure 4.3. SEM images of S2 with (a) X50 (b) X100 (c) X150 (d) X200.

Figure 4.4. Micro-CT images after image processing and counted glass fibers of (a) S1 and (b) S2.

Figure 4.5. Probability distribution function of (a) S1 and (b) S2 with theoretical modeling function of Weibull, Lognormal and GEV distribution function.

Figure 4.6. Cumulative distribution function of (c) S1 and (b) S2 with theoretical modeling function of Weibull, Lognormal and GEV distribution function.

Figure 4.7. Probability function of (a) S1 and (b) S2 with theoretical modeling function of Weibull, Lognormal and GEV distribution function.

Figure 4.8. (a) A tensile test piece from a resin composite material of the LCP (red rectangular indicates a taken section)

Figure 4.9. (b) 3D construction of S1 tensile specimen.

Figure 4.10. (c) 3D construction of S2 tensile specimen.

Figure 4.11. Numerical analysis and Injection moling in sprial channel of S1 at 340 °C.

Figure 4.12. Numerical analysis and Injection moling in sprial channel of S1 at 360 °C.

Figure 4.13. Numerical analysis and Injection moling in sprial channel of S1 at 380 °C.

Figure 4.14. Numerical analysis and Injection moling in sprial channel of S2 at 340 °C.

Figure 4.15. Numerical analysis and Injection moling in sprial channel of S2 at 360 °C.

Figure 4.16. Numerical analysis and Injection moling in sprial channel of S2 at 380 °C.

Figure 4.17. Comparison of distance length of S1 and S2 at each temperature.

Figure 4.18. Numerical analysis results of (a) S1 and (b) S2 under slow flow rate.

Figure 4.19. Numerical analysis results of (a) S1 and (b) S2 under fast flow rate with real images and Micro-CT images.

Figure 4.20. The ratio of mass differences as a function of temperature.

Figure 4.21. Numerical analysis results of (a) S1 and (b) S2 with same

thermal conductivity coefficient ($0.9 \text{ W/m } ^\circ\text{C}$).

Figure 4.22. Numerical analysis results of (c) S1 and (d) S2 with same thermal conductivity coefficient ($1.8 \text{ W/m } ^\circ\text{C}$).

Figure 4.23. Numerical analysis results of (e) S1 and (f) S2 with same thermal conductivity coefficient ($2.5 \text{ W/m } ^\circ\text{C}$).

Figure 4.24. Numerical results of S1 with different value of n (a) 0.6 (b) 0.8 (c) 1.

Figure 4.25. Numerical results of S2 with different value of n (a) 0.6 (b) 0.8 (c) 1.

Figure 4.26. Images of Micro-CT, real micro connector and 3D construction of fiber clogging problem at the top part of micro connector and line spectrum of intensity.

Figure 4.27. Images of Micro-CT, real micro connector and 3D construction of fiber clogging problem on the side part of micro connector and line spectrum of intensity.

Figure 4.28. Images of Micro-CT, real micro connector and 3D construction for fully filled micro connector and line spectrum of intensity.

Figure 4.29. Longitudinal direction of effective elastic modulus as a function of ratio of glass fiber and total volume fraction with theoretical models for S1 and S2. The inset graph represents elastic modulus of S1, S2 and reference sample.

Figure 4.30. Transverse direction of effective elastic modulus as a function of ratio of glass fiber and total volume fraction with theoretical

models for S1 and S2.

Figure 4.31. Probability distribution function with various log location parameters and log scale parameters.

Figure 4.32. Theoretical effective elastic moduli along the longitudinal direction.

Figure 4.33. Theoretical effective elastic moduli along the transverse direction.

Figure 4.34. Tensile stress curves of S1, S2 and a reference sample with respect to tensile strain.

Table 1. Coefficient of Thermal Expansion (CTE) results of S1 and S2.

Table 2.1. The relevant distribution parameters of S1.

Table 2.2. The relevant distribution parameters of S2.

Table 3. Residue weight percent of each section at same temperature.

I. INTRODUCTION

1.1. Overview of injection molding

Injection molding has been considered most efficient polymer processing method to fabricate from a large size of product such as a bumper of car or a bezel of television to a micro size of chip or connector for electronic devices as well as complex shaped product and capability of mass production. Since the products tend to miniaturize, the micro injection molding became one of the key method for micro-scale product [1]. In case of manufacturing a micro size of product, it is very important to control of flowability of materials due to high shear rate, solidification rate and viscosity. Generally, liquid crystalline polymer (LCP) has been widely used for injection molding because it has good processability because of a rigid rod within materials [2]. Moreover, it is well known that LCP has very low melt viscosity which leads good processability during injection molding process and minimize the defect from breakage [3]. Low viscosity compared with isotropic liquid is considered one of the unique properties of LCP and this property comes from the ready

orientation of the LC molecules during flowing process. However, since the orientation of LCP has resulted in rheological property show anisotropic properties [4] therefore, there should be a particular inclusion to reduce the anisotropic property. Reinforced composites have improvement in mechanical property and decrease anisotropic characteristic, on the other hand, reinforced composites have decreased flowability. In this sense, it is important to understand the flowability depends on properties of inclusions.

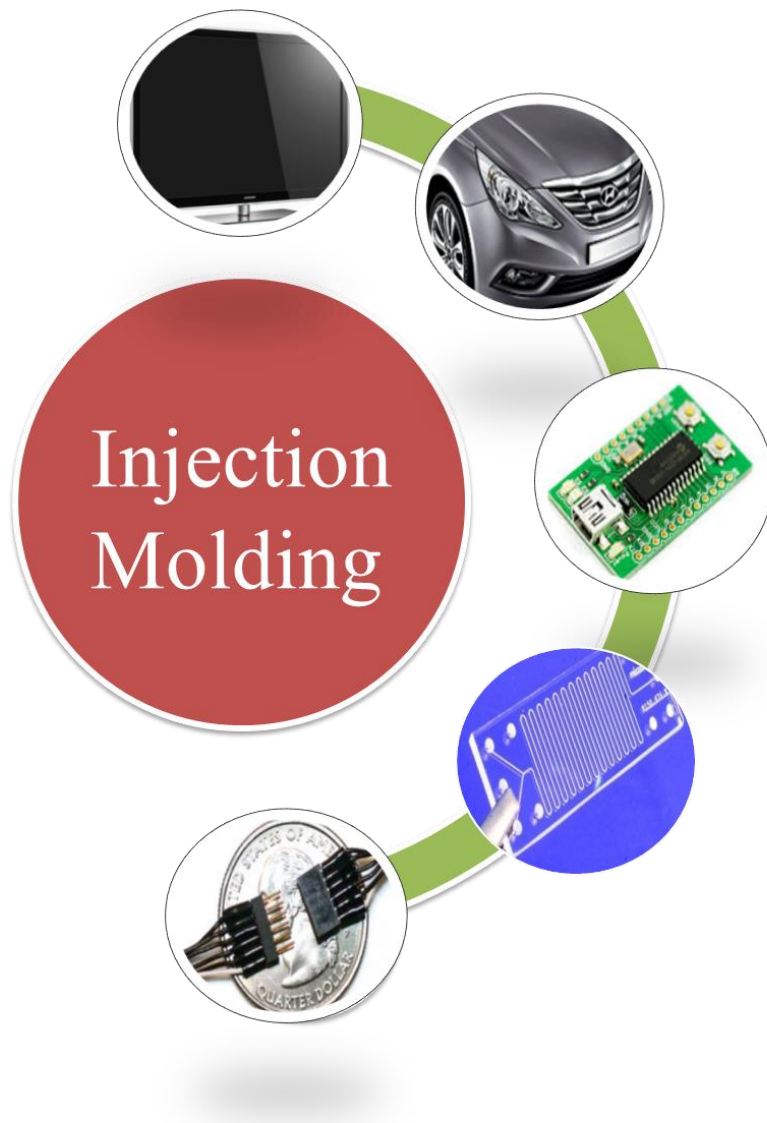


Figure 1. Overview of injection molding

1.2. Overview of FLD and Micro-CT

Characteristic of composites varies according to their properties of contained materials such as length and orientation of fibers, the ratio of the glass fibers and minerals as well as the species of included materials [5-7]. Several methods have been developed so far to observe the fiber length distribution (FLD) such as confocal laser scanning microscopy [8-10]. However confocal laser scanning microscopy is not good enough to analyze the length of fiber distribution for complex shape geometries in three-dimensional images due to its low resolution. It is possible to obtain 3D information of FLD with high resolution in a non-destructive way [11, 12] by using Micro-CT [13, 14]. In general, X-ray Micro-CT is a method for generating a three dimensional image by stacking a large number of 2D cross section images, thus this technique can be applied in various fields to investigate the internal structure such as, damaged areas [15], porosity[16] and bone microstructure for medical purpose [17]. FLD enables us to anticipate the property of materials since the fiber length is the key factor in determining the mechanical property [18-20], electrical property [21], and thermal property of materials

[22-24]. Furthermore, FLD influences the processability of composites because it varies with rheological behavior such as flowability and viscosity [25, 26]. Besides FLD, estimation of the species and amount of content in the material also plays an important role in understanding the rheological behavior [27-29]. Therefore, in order to understand the characteristic of the mixed materials, components analysis of the material is necessary. In this study, we obtained the images of tensile specimens by using Micro-CT with high resolution, then reconstructed the three dimensional data to visualize into probability distribution function. The theoretical analysis of flowability, i.e., processability is presented and the theoretical analysis results were compared with the experimental results. In the last of this study, a fiber clogging problem on the side and on the front tip of micro connector was analyzed through 3D constructed images, Micro-CT images, and the real pictures of micro connector.

1.3. Objective of this work

In this study, for comprehensive understanding viscosity affected by volume fraction, FLD and thermal conductivity is prior object to investigate flowability and processability in micro scale of molded part. We used two kinds of LCP based on different properties of inclusions. First of all, incineration experiment and Scanning electron microscope (SEM) experiment were taken to verify volume fraction and observe length of glass fiber visually. Second of all, for quantitative analysis of FLD, Micro-CT and image processing were performed then, the results were transferred theoretical models and 3D structures. Finally, numerical analysis results were characterized by commercial software MOLDFLOW. The numerical analysis and experiments both indicated that a fiber clogging problem was observed in a micro sized path. Particularly, we focused on the influence of FLD in micro sized of connector under various conditions such as flow rate, thermal conductivity.

II. THEORETICAL BACKGROUND

2.1. Parameters effect on viscosity

The variables related to viscosity are generally classified into 3 types: volume fraction, FLD and thermal conductivity.

2.1.1. Volume fraction

The volume fraction is one of the critical parameter determined the viscosity [30]. Generally, the composite which contains more glass fiber inside has a relatively worse viscosity since glass fiber can act as an obstacle during micro injection molding process. Therefore, the composite with lower volume fraction can flow the narrow path without interruption. However, there are certain drawbacks associated with the decrease of volume fraction. Typically, the lower volume fraction of composite increases flowability and reduces mechanical property at the same time thus, both the rheological property and mechanical property can be determined how much volume fraction of inclusion such as glass fiber is included in the materials. For this reason, when the micro-chip or micro-connector were fabricated by using injection molding process, it is necessary to

optimize the weight percent of volume fraction because fabricated appliances with less volume fraction of inclusions than it is needed can have well-formed shape, on the other hand, it might not be appropriate to use due to poor mechanical property.

2.1.2. Fiber Length Distribution (FLD)

Another important parameter which influences on the viscosity is a FLD. During the micro injection molding process, the fiber clogging problem is frequently occurred problem which increases the probability to manufacture defected appliances. Since the length of glass fiber included in LCP is approximately up to 1000 μ m, it is long enough length to block the stream of the rest of material during injection molding particularly at the few milli-meters sized narrow path. Consequently, consideration of the length of glass fiber, of course, its distribution have become more and more important when the micro-scale of product like micro-connector and micro-chip are designed. Thus, it can be suggested that FLD influences on the viscosity considerably which serve as a base to anticipate the flowability.

2.1.3. Thermal conductivity

Usually, solidification rate is significantly affected by heat transfer between mold temperature and melt temperature which means that under the same temperature of mold, the solidification rate should be defined based on the thermal conductivity of inclusions within the material. This suggests that, the glass fiber which has higher thermal conductivity can transfer heat between mold and materials relatively quickly then, it would be solidified. Therefore, under the same condition, it is difficult to flow the path before filling the mold fully.

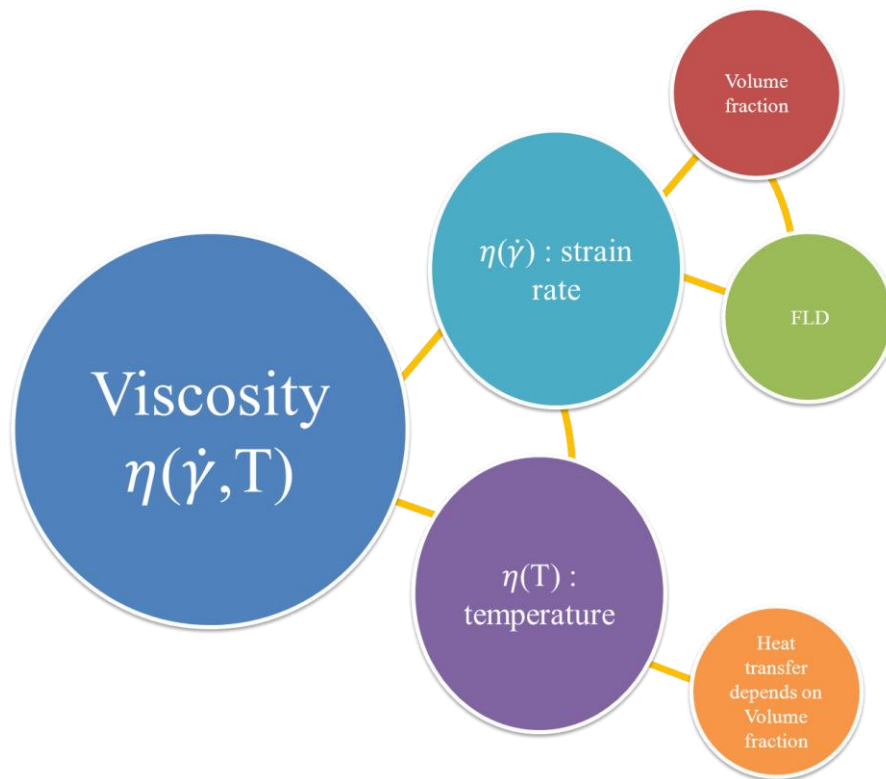


Figure 2. Parameters influence on the viscosity.

2.2. Theoretical models

In this study, three types of statistical modeling, i.e. Weibull distribution function, Lognormal distribution and the generalized extreme value (GEV) were used for comparison with experimental distribution functions. Equations are as followed.

2.2.1. Weibull distribution function

$$F(x; \kappa, \lambda) = \begin{cases} \left(\frac{\kappa}{\lambda} \left(\frac{x}{\lambda} \right)^{\kappa-1} e^{-\left(\frac{x}{\lambda} \right)^{\kappa}} \right) & x \geq 0 \\ 0 & x < 0 \end{cases}$$

Where, κ and λ are shape parameter, scale parameter, respectively.

2.2.2. Lognormal distribution function

$$F(x; \mu, \sigma) = \frac{1}{x\sigma\sqrt{2\pi}} e^{-\frac{(\ln x - \mu)^2}{2\sigma^2}}, \quad (x > 0)$$

The μ and σ represent log location parameter and log scale parameter, respectively.

2.2.3. The generalized extreme value (GEV) function

$$F(x;\mu,\sigma,\xi) = \frac{1}{\sigma} t(x)^{\xi+1} e^{-t(x)}, \quad t(x) = \begin{cases} \left(1 + \left(\frac{x-\mu}{\sigma}\right)\xi\right)^{-\frac{1}{\xi}} & \text{if } \xi \neq 0 \\ e^{-(x-\mu)/\sigma} & \text{if } \xi = 0 \end{cases}$$

The μ , σ and ξ are location parameter, scale parameter and shape parameter, respectively

2.3. Generalized Newtonian fluid model

2.3.1. Cross-WLF model

In order to analysis numerically, the Cross-WLF equation was applied, since viscoelastic behavior is complicate to get the solution, instead of viscoelastic model, we use the generalized Newtonian fluid model in this study. The Cross-WLF equation is given by

$$\eta = \frac{\eta_0}{1 + \left(\frac{\dot{\gamma} \eta_0 \gamma}{\tau^*} \right)^{1-n}}$$

where η is the melt viscosity (Pa s), η_0 the zero shear viscosity, $\dot{\gamma}$ the shear rate (1/s), τ^* the critical stress level at the transition to shear thinning, n the power law index.

III.EXPERIMENTS

3.1. Sample characterization

3.1.1. Materials

Two types of composites were prepared and investigated in this study: S471 and S475 (Polyplastics, Vectra S471 and Vectra S475) included with glass fibers and minerals were used as base composites. S471 and S475 are denoted S1 and S2, respectively. Both composites were available in the form of cylindrical pellets. Besides S471 and S475, micro connector was used which was made of S471 to analyze the processability, i.e, flowability. Tensile specimens were fabricated by an injection molding machine, then measured by Micro-CT to determine FLD [14].

3.1. Overview of analysis methods

3.2.1. Incineration

In this study, 3g of the cylindrical pellets were placed into a squared crucible and heated at 600°C for 24 hours in the stream of air in a furnace (Nabertherm GmbH), then, the rest of the weight was

measured in ash to calculate the weight fraction of included glass fibers and minerals.

3.2.2. Thermo Gravimetric Analysis (TGA)

The thermo gravimetric analysis (TGA) was performed using TA instruments TGA 2950, and the ratio of mass differences of indefectible GB045 and short-shot GB045 micro-connector divided into each two parts were evaluated as a function of temperature. The samples were heated from 30 °C to 800 °C, then, the mass differences were evaluated at the same temperature.

3.2.3. Thermo Mechanical Analyzer (TMA)

Thermo Mechanical Analyzer (TMA) was employed by TMA equipment (TA instruments Q400) to acquire to information of coefficient of thermal expansion (CTE) of S1 and S2. The temperature rate is 5 °C / min in the temperature range 23 °C to 230 °C. Rectangular shaped small size of samples (4mm x 10mm, width and length) for both flow direction and transverse direction of orientation of inclusions were prepared by using laser cutter (jg10060).

3.2.4. Scanning Electron Microscope (SEM)

The Scanning electron microscope (SEM) method is one of the more practical ways of observing a surface of materials. Surface analysis was carried out with Field-Emission Scanning Electron Microscope (FE-SEM, JSM-7600F) with 50~200 times magnification, 5kV of acceleration voltage and 8mm of working distance (WD). Each specimen was coated before SEM examination.

3.2.5. Micro-CT imaging and image processing

Micro-CT system (Skyscan, 1172) with high resolution was used to explore the micro structure of the glass fiber and minerals within composites. Source voltage was 100 kV, which was powerful enough for tomography to obtain 3D images. The data from Micro-CT were analyzed quantitatively by using a commercial image analysis tool (Media Cybernetics, Image-Pro Plus 6.0). After image processing, the probability distribution function graph for graphical visualization was obtained by numerical method of Matlab toolbox. For better visual analysis, images from Micro-CT were combined for three-

dimensional structure. A commercial image tool (image j) was used to reconstruct 3D images.

3.2.6. Flowability test

A metal spiral shaped mold with 650 μ m in height, and with 1500 μ m in a fine channel width of a metal mold was fabricated to measure the flowability of S1 and S2. A flow length which indicates the flowability while the resin is flowing through the spiral channel at different temperatures was compared with the results of numerical analysis by using a commercial tool (Autodesk Moldflow).

3.2.7. Universal testing machine (UTM)

Elastic moduli of samples were examined by using a universal testing machine (UTM) (Instron, 8801) with 5 mm/min of the crosshead speed according to ASTM D638 for tensile testing.



Figure 3. Image of spiral channel.

IV. RESULTS AND DISCUSSION

4.1. Anisotropic property of LCP

General understanding of the anisotropic property of LCP should be taken prior to decide the optimal process condition of injection molding since anisotropic property might cause distortion. It is well known fact that LCP appears anisotropic property, thermal expansion is examined by TMA. It can be seen from the data in Table 1. Flow direction of CTE values for S1 and S2 are much lower than the transvers direction of CTE values because, in general, LCP has a molecular orientation along flow direction.

Table 1. Coefficient of Thermal Expansion (CTE) results of S1 and S2.

CTE(Coefficient of Thermal Expansion) ($10^{-6}/^{\circ}\text{C}$)		
	Flow direction	Transverse direction
S1	7.049	104.4
S2	24.07	66.34

4.2. Volume fraction and morphological analysis

4.2.1. Incineration

The weight fraction of glass fibers and minerals included in S1 and S2 are shown in Figure 4. The weight fraction of the inorganic inclusions is defined as:

$$\text{Weight fraction (\%)} = \frac{w_0 - (w - w')}{w_0} \times 100 \quad (1)$$

where, w_0 is the weight of original sample, w is the weight of crucible plus original sample and w' is the weight of crucible plus ash after incinerating the sample. As a result, the total weight fraction of inclusion in S1 and S2 was confirmed as 44.17 % and 30.65%, which indicates that S1 has more glass fiber and mineral than S2, and that it is envisaged each composite system consisted of S1 and S2 may have different rheological and thermophysical properties, i.e, different flowability associated with different transition temperature and viscosity [31], moreover, higher volume fraction in S1 could be

attributed to lower flowability because glass fiber acts as an obstacle in channel.





S1		S2	
Before Incineration	After Incineration	Before Incineration	After Incineration
			
Inclusions : 44.17 %		Inclusions : 30.65 %	

Figure 4.1. Incineration result of S1 and S2 with volume fraction of glass fibers and minerals.

4.2.2. Morphology analysis

The results obtained from the surface analysis by using SEM are presented Figure 4.2 and Figure 4.3 with various magnifications. There was a significant difference between the two specimens. As can be seen from the Figure 4.2 and Figure 4.3, the S1 reported significantly longer glass fiber length than the S2. Moreover, what is interesting in these images is that not only the S1 has a longer glass fiber but also it contains more amounts of glass fibers than that of S2, which is a coincident result with incineration results above. These incineration experiment and surface analysis enable us to anticipate the flowability. The length of glass fibers in the SEM image of S1 are approximately 300 μ m, thus, these glass fibers could get tangled at narrow path and act as hindrances.

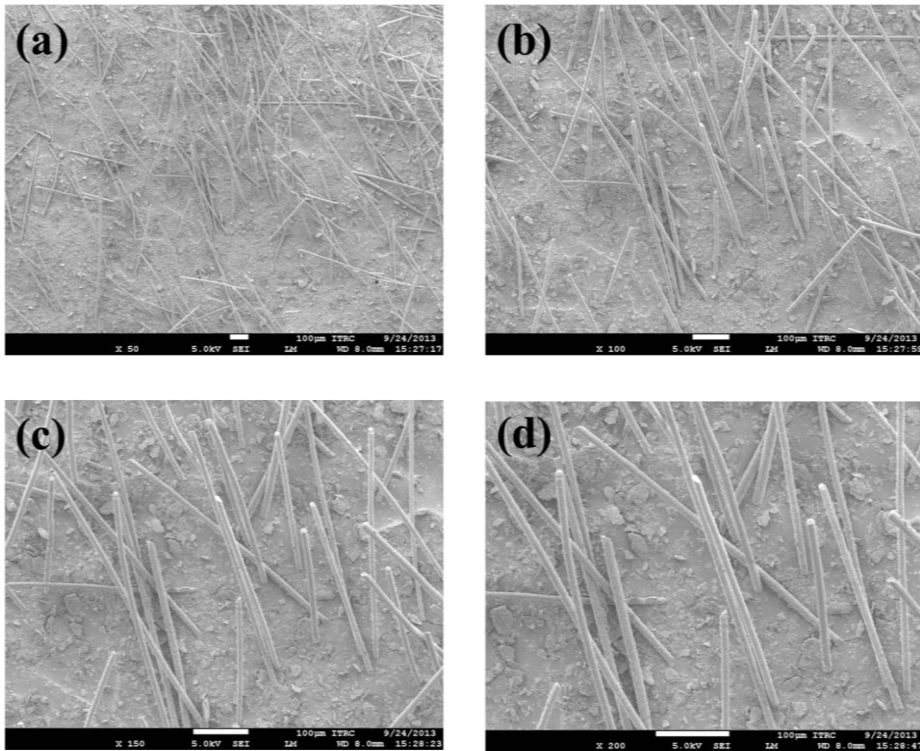


Figure 4.2. SEM images of S1 with (a) X50 (b) X100 (c) X150 (d) X200.

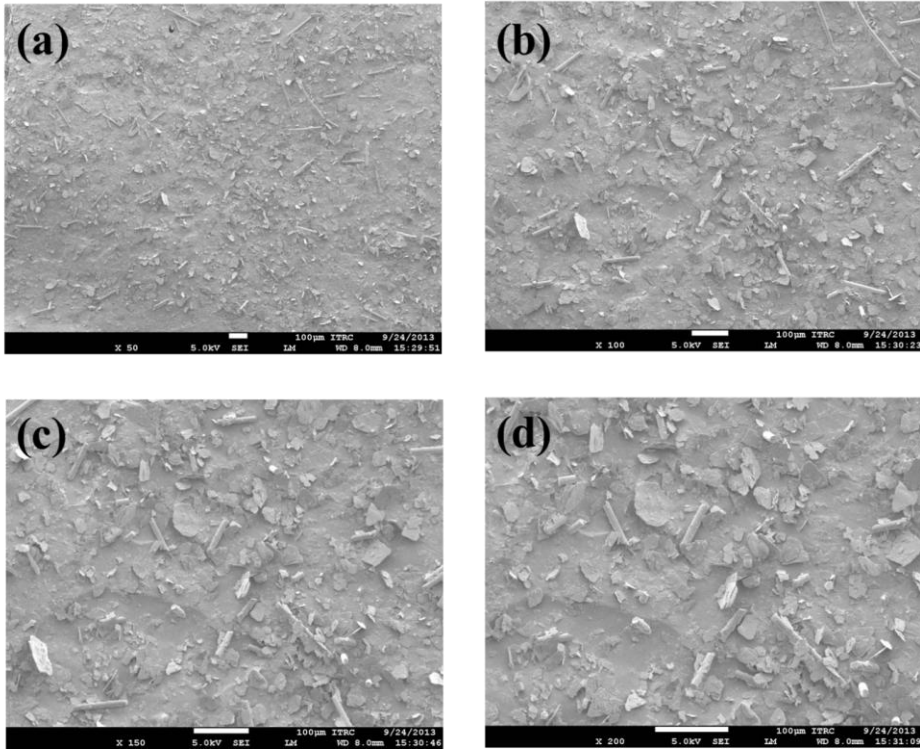


Figure 4.3. SEM images of S2 with (a) X50 (b) X100 (c) X150 (d) X200.

4.3. Quantification of fiber length distribution

4.3.1. Image processing

It is worthy to note that FLD becomes significantly important as manufacturing micro-devices, micro-structures, and micro-molded parts since the channel path or pitch in the micro-sized products is on the order of tens of micron to hundreds of microns which is comparable to the length of inclusions. Therefore, the quantification of FLD should be realized prior to investigating the fluidic properties of molten polymer composites. In this sense, morphological characterization of both S1 and S2 was conducted so as to quantify the FLD in each sample as shown in Figure 4.2 and Figure 4.3. It is shown that fiber length of S1 seems to be longer than that of S2. However, it needs more accurate, reliable, and rich data set to assess the distribution of fiber length. For better understanding of FLD, Micro-CT was used to quantitatively analyze the internal structure of S1 and S2, and then image processing was conducted by using commercial software (Media Cybernetics, Image-Pro Plus 7.0). A thin tensile specimen (10 mm in width x 1 mm in height) was produced to induce the unidirectional fiber orientation along the flow direction.

The images from Micro-CT pictures were filtered to emphasize the horizontal direction of glass fibers, and then the total number of detected glass fibers was counted. It is apparent that the length of glass fibers in S1 is longer than that of S2 as shown in Figure 4.4a and Figure 4.4b.

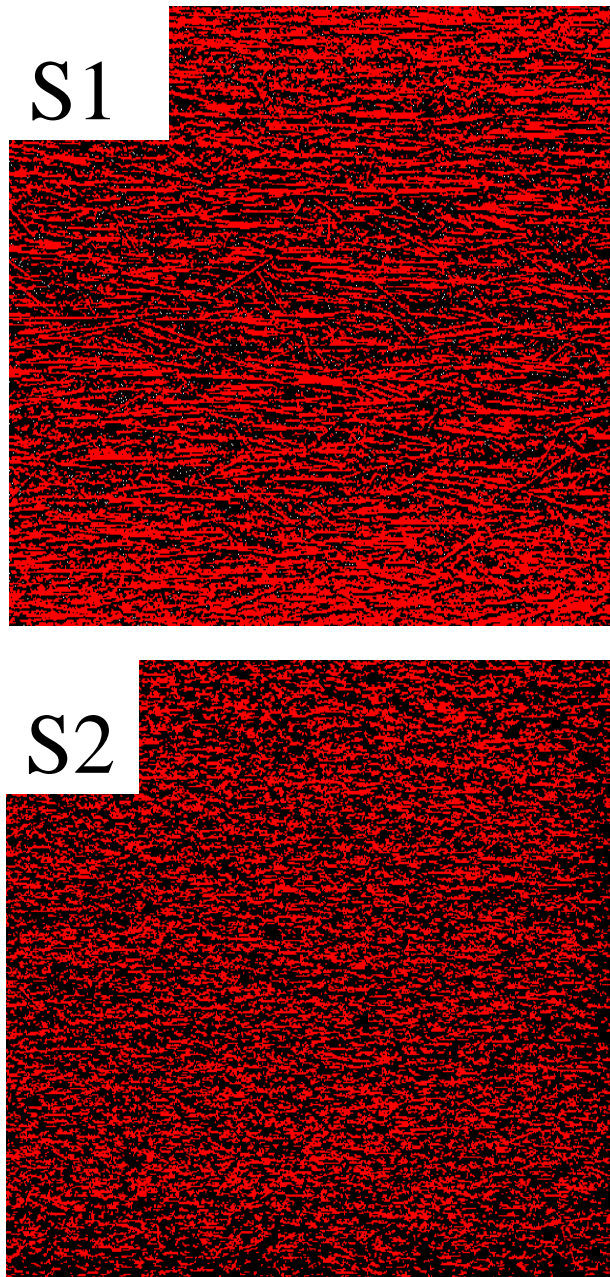


Figure 4.4. Micro-CT images after image processing and counted glass fibers of (a) S1 and (b) S2.

4.3.2. FLD & Theoretical analysis

The number the counted glass fibers from image process (Figures 4.4) were described into probability density function, cumulative probability function and probability function as a function of length of glass fibers with theoretical models. The difference of distribution between S1 and S2 is obvious from the results of probability distribution function that the length of glass fibers in S1 was distributed ranging from 10 to 1000 μm , however, the length of glass fibers in S2 ranges up to 500 μm (Figure 4.5a and Figure 4.5b). This is similar result compared with the results from SEM images, hence, it is verified that S1 has longer glass fibers in quantitatively and visually. The cumulative probability functions and probability functions also support that S1 has larger length distribution than S2 (Figure 4.6 and Figure 4.7). As shown in Figure 4.6 and Figure 4.7, near 1000 μm length of glass fibers exist in S1. From the probability distribution function, it is found that the GEV function is most coincident with experimental results, which means that the GEV function is appropriate statistical model to anticipate the distribution of inclusions. This behavior is also represented as can be seen from

the Figure 4.6 and Figure 4.7, among the theoretical models the GEV gives a reasonable explanation where glass fibers are shorter than 300 μm .

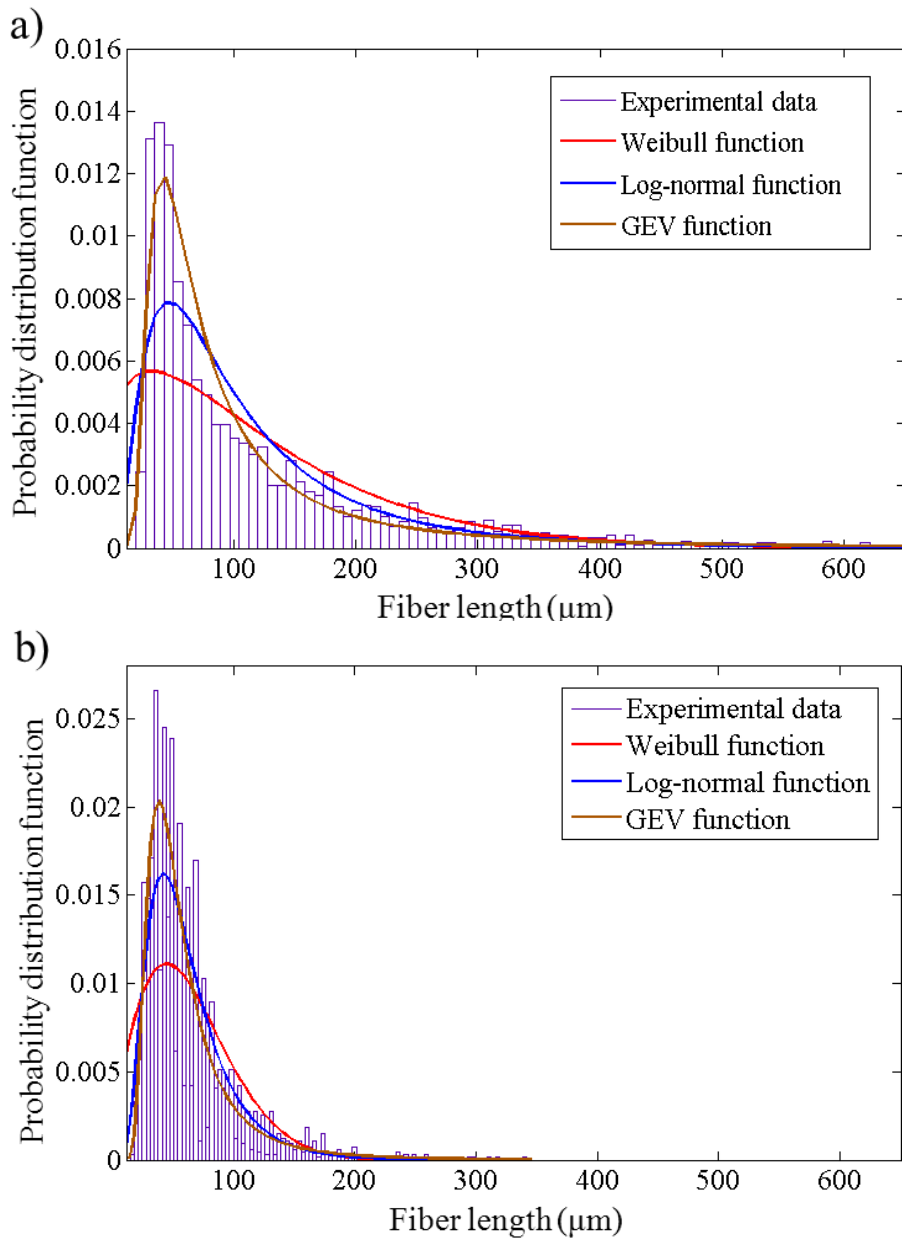


Figure 4.5. Probability distribution function of (a) S1 and (b) S2 with theoretical modeling function of Weibull, Lognormal and GEV distribution function.

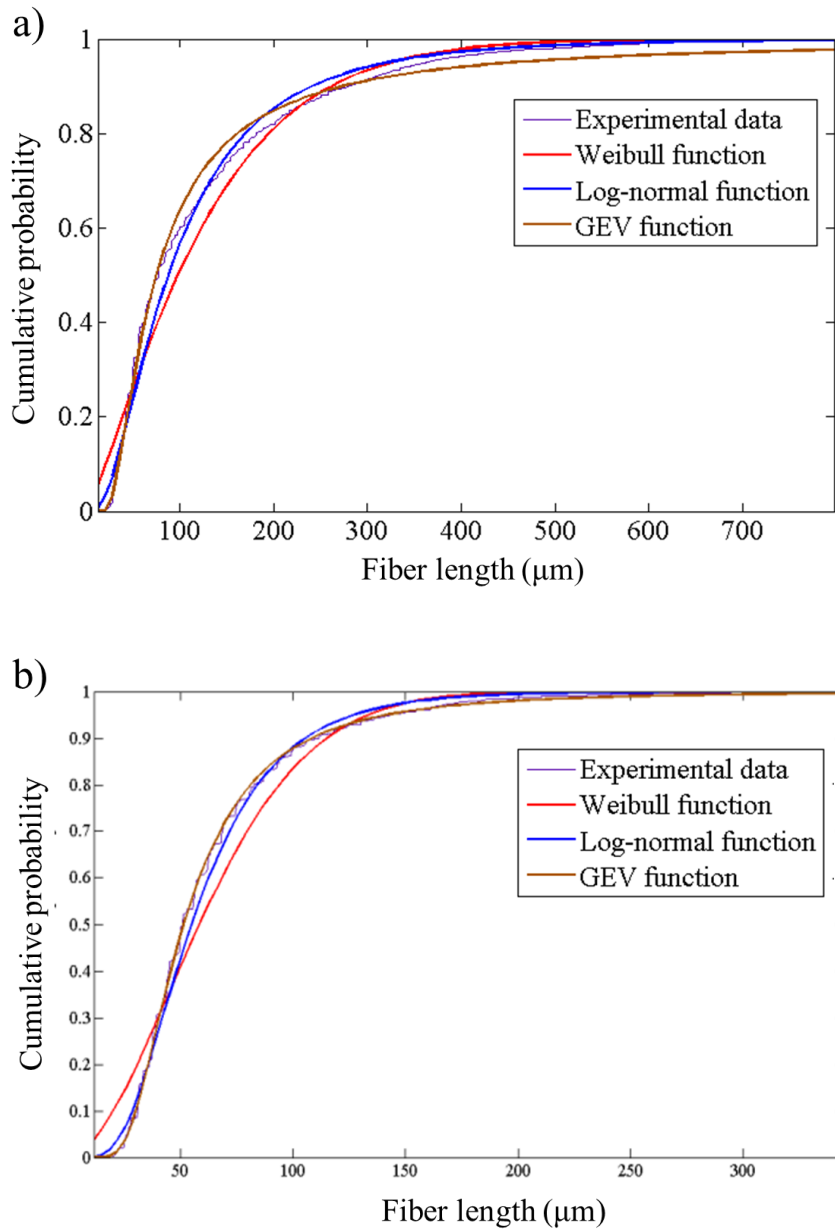


Figure 4.6. Cumulative distribution function of (a) S1 and (b) S2 with theoretical modeling function of Weibull, Lognormal and GEV distribution function.

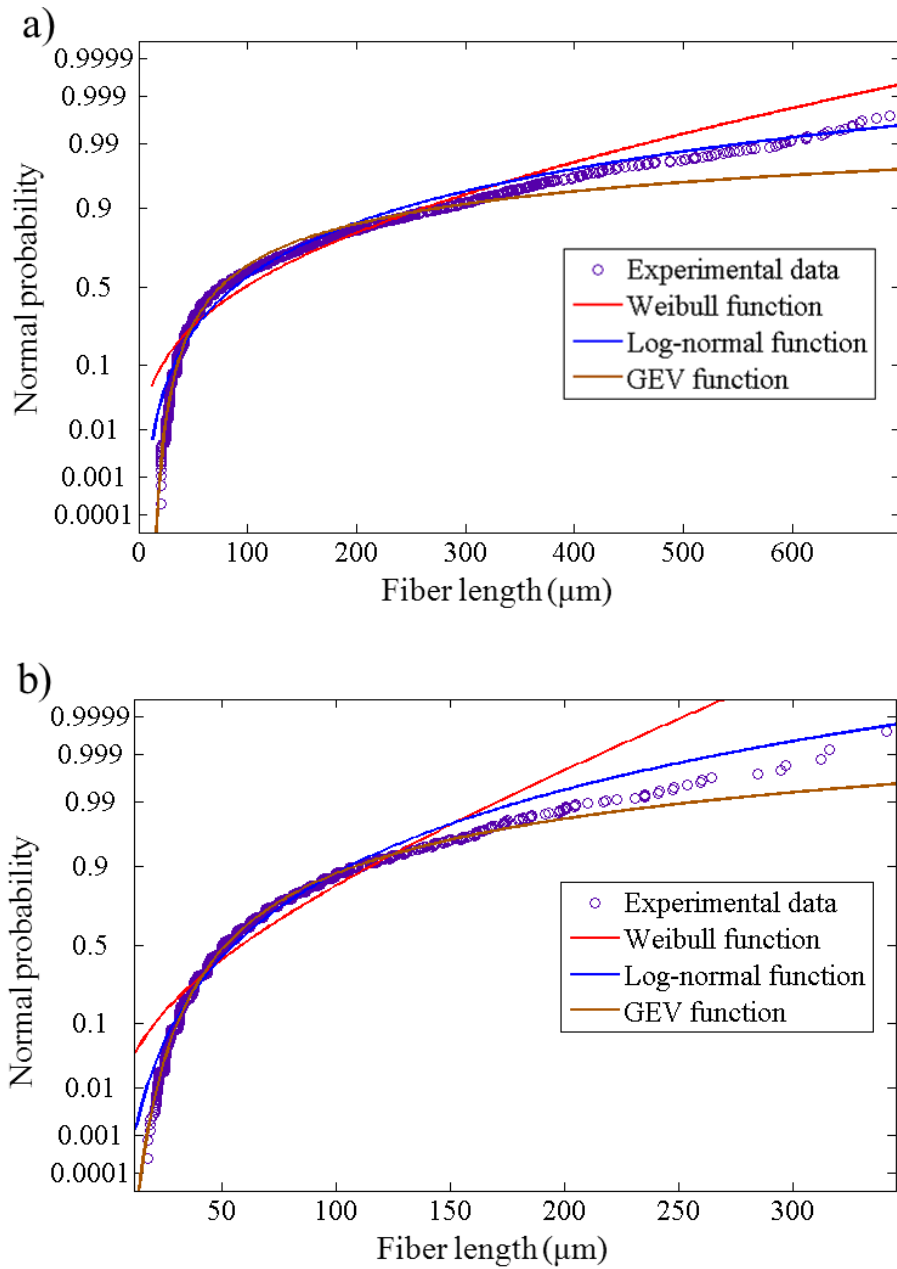


Figure 4.7. Probability function of (a) S1 and (b) S2 with theoretical modeling function of Weibull, Lognormal and GEV distribution function.

Table 2.1. The relevant distribution parameters of S1.

S1	Weibull	Log normal		GEV	
	$\lambda_{(\text{scale})}$	181.18	$\mu(\log$ location)	4.70893	$\xi(\text{shape})$ 1.34238
	$\kappa_{(\text{shape})}$	0.949429	$\sigma(\log$ scale)	0.914881	$\sigma(\text{scale})$ 33.422
				$\mu(\text{location})$	60.7034

Table 2.2. The relevant distribution parameters of S2.

S2	Weibull	Log		GEV	
		normal			
	λ (scale)	124.151	μ (log location)	4.513	ξ (shape) 0.715737
	κ (shape)	1.51807	σ (log scale)	0.579383	σ (scale) 27.3907
					μ (location) 65.8703

4.3.3. FLD & 3D structure

In order to investigate the 3D fiber architecture, volumetric reconstruction was performed using an image processing method. A Tensile specimen was fabricated shown as Figure 4.8 with 1mm of thickness. Because of its thin thickness, glass fibers are well oriented along the flowing direction within the tensile test sample. Then, the tensile specimens were observed by using high resolution of Micro-CT for image processing. For better visualization, images of each plane were enhanced by controlling the contrast and brightness, transformed into binary images by a thresholding method, and then stacked altogether. It was confirmed that most of glass fibers were oriented along the flow direction for both S1 and S2. The volumetric reconstruction shows clearly that S1 has longer fibers than S2 in the whole 3D volume representing the observation by using Micro-CT can verify FLD as well as fiber orientation effectively.

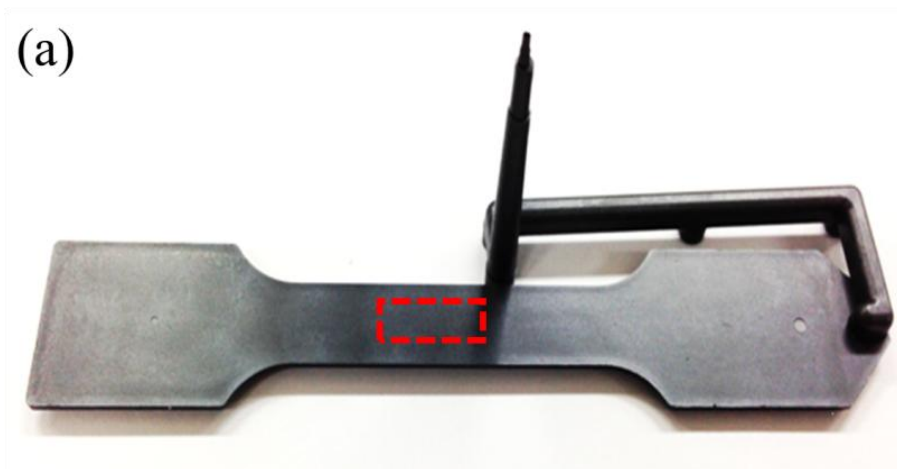


Figure 4.8. (a) A tensile test piece from a resin composite material of the LCP (red rectangular indicates a taken section)

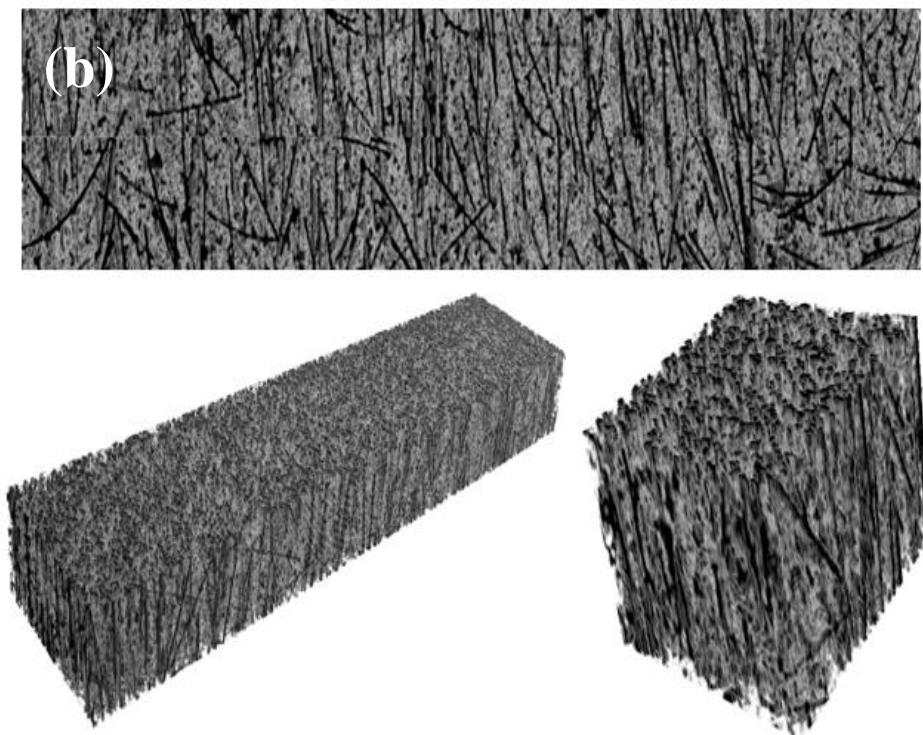


Figure 4.9. (b) 3D construction of S1 tensile specimen.

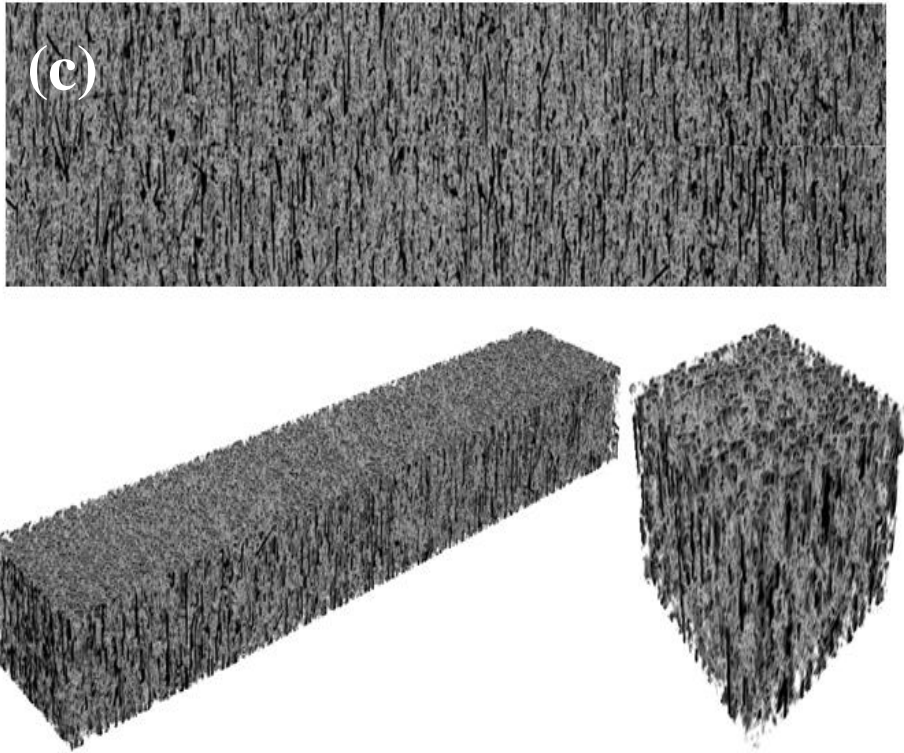


Figure 4.10. (c) 3D construction of S2 tensile specimen.

4.4. Injection molding & Numerical Analysis

4.4.1. Flowability results in Spiral Channel

It is worthy to note that the flowability strongly depends on kinds of polymeric materials. We fabricated a spiral shaped mold with 650 μm in height and 1500 μm width to measure the flowability of each sample. A Flow length indicates the distance that molten polymer flows through the spiral channel. It must be kept in mind that there are two main reasons for different flowability in micro-molded parts as using inclusion reinforced materials: first, the viscosity of polymeric materials and second, the hindrance of flow on account of reinforcements. It is already known that the viscosity of liquid crystalline polymer is strongly dependent on temperature [32, 33] because of the thermal conductivity and volume fraction within the material. Therefore, it is expected that the flowability of S2 would be better than S1 since the viscosity of S2 is lower than that of S1 at the same temperature. In case of S2, the dependence on viscosity in regard to temperature appears significant, so that the flowability is expected to be increased more clearly than S1 as temperature increases. It is believed that in the case of S2, since the amount of

contained material is less than S1 in the resin and the length of the glass fibers is shorter than the S1, the decrease in flowability of the resin is relatively small. It is shown that the flow lengths of S1 and S2 increase as temperature increases and the increase is large when temperature raises from 340 °C to 360 °C than from 360 °C to 380 °C, which is associated with that fact that the melting temperature of LCP is about 340 °C ~ 350 °C. Consequently, S2 has greater flowability than S1 in a spiral channel. It is useful to employ the spiral channel since the effect of viscosities of polymeric materials on the flowability can be evaluated. However, the spiral channel is not the typical cases for micro-molded parts in that micro-pitches, pinched channels, or branched capillary channels are not considered. Therefore, flowability may be different when a micro-molded part has lots of small channels. From the point of view of the effect of viscosities, S2 has a longer flow distance since in the case of S1, it is solidified faster than S1 before it filled the narrow micro channel. In this sense, reinforcing fillers hinders the flow through the narrow channels and junctions. Therefore, S2 is completely filled while S1 is not filled since S2 has lower amount of fillers and shorter fiber length than those of S1.

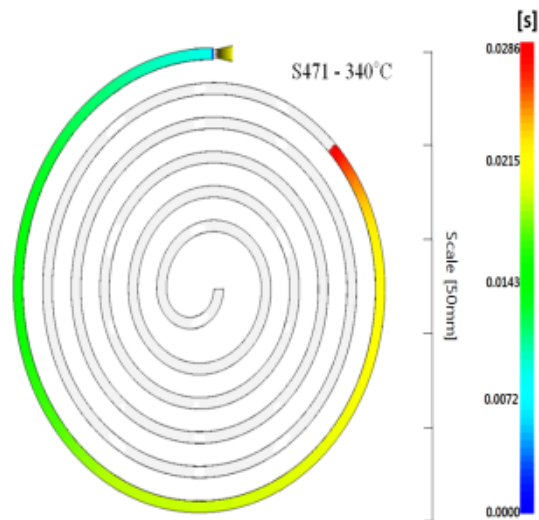


Figure 4.11. Numerical analysis and Injection molding in spirial channel of S1 at 340 °C.

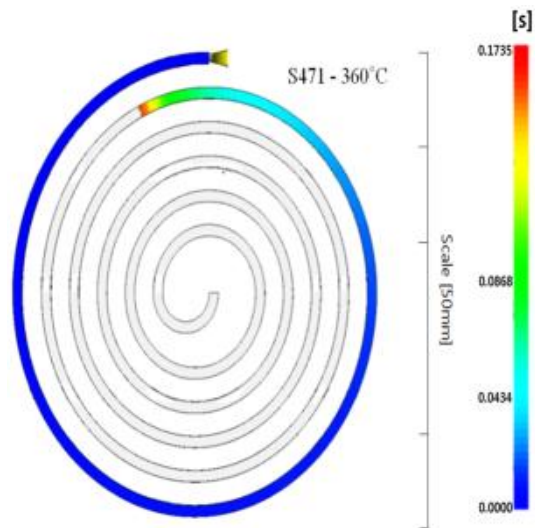


Figure 4.12. Numerical analysis and Injection molding in spirial channel of S1 at 360 °C.

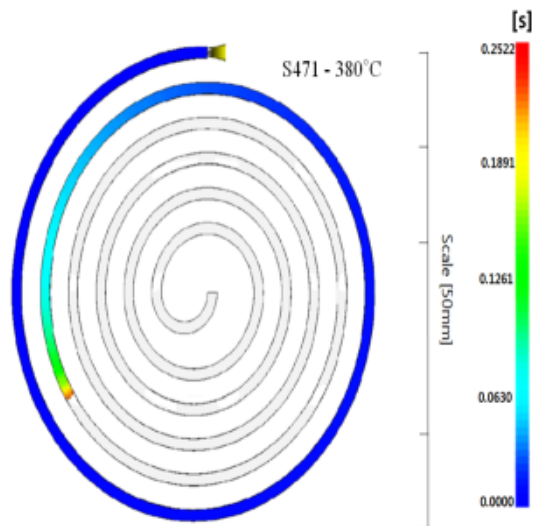


Figure 4.13. Numerical analysis and Injection molding in spirial channel of S1 at 380 °C.

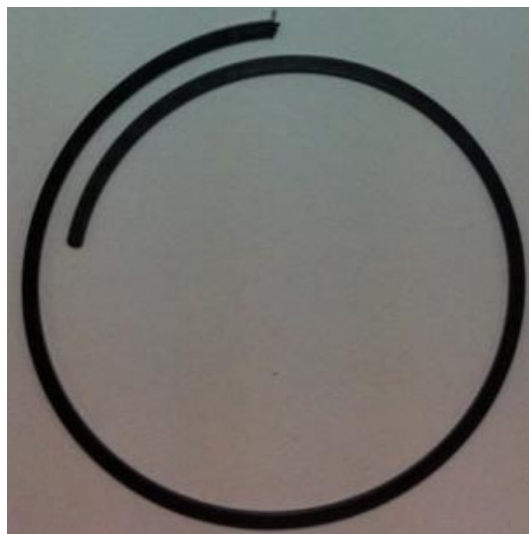
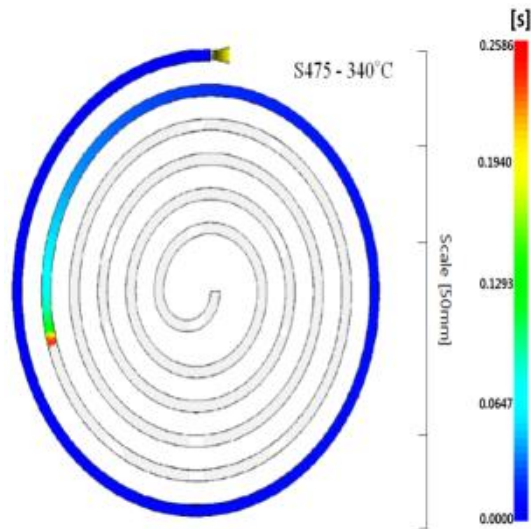


Figure 4.14. Numerical analysis and Injection molding in spirial channel of S2 at 340 °C.

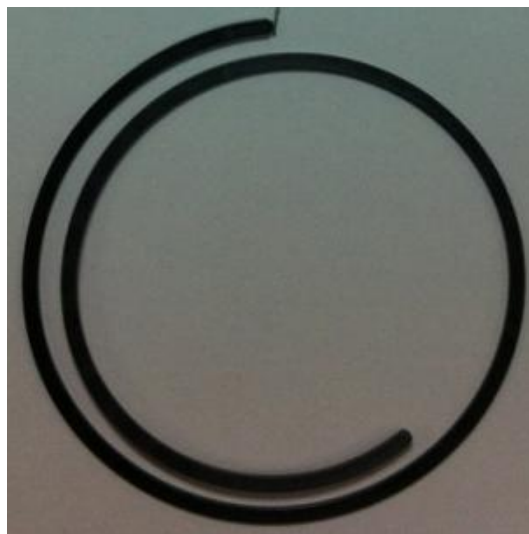
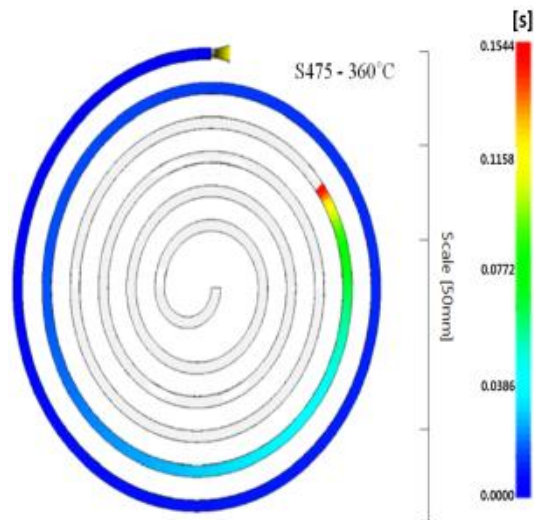


Figure 4.15. Numerical analysis and Injection molding in spirial channel of S2 at 360 °C.

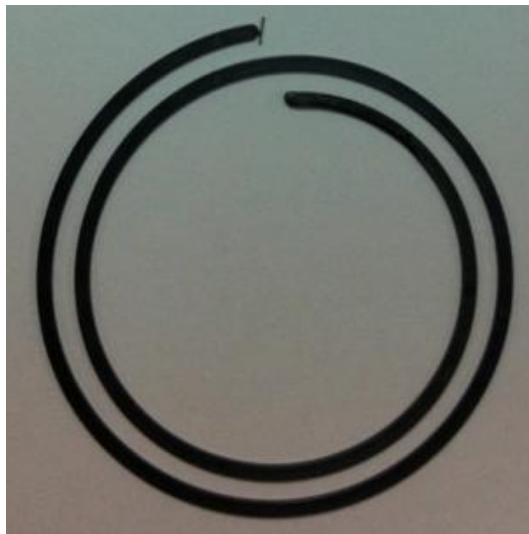
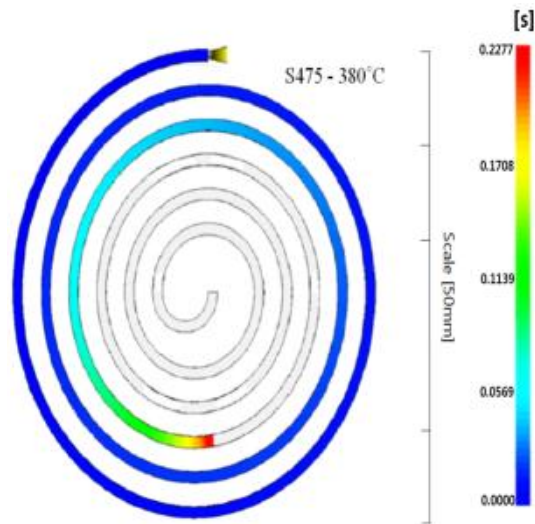


Figure 4.16. Numerical analysis and Injection molding in spirial channel of S2 at 380 °C.

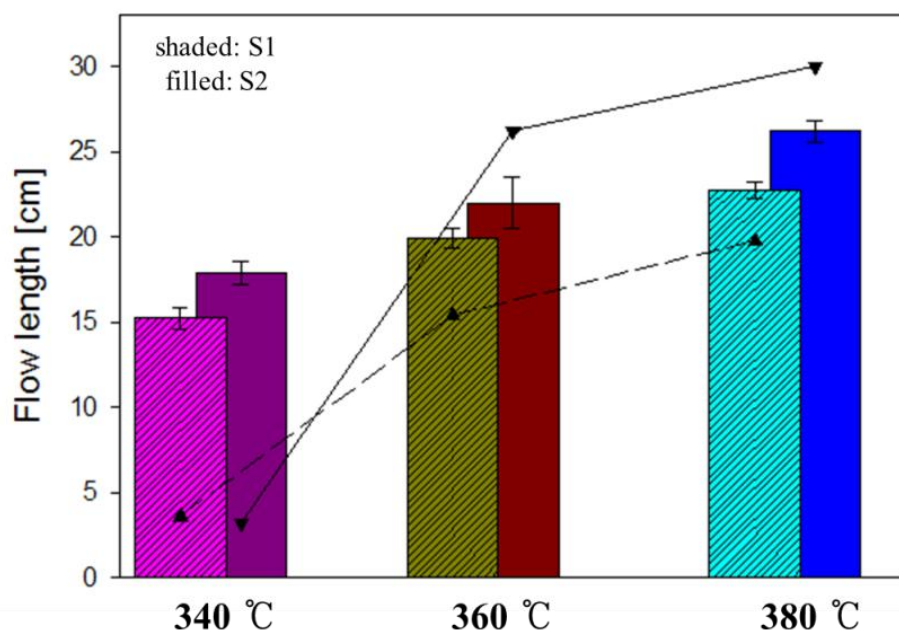


Figure 4.17. Comparison of distance length of S1 and S2 at each temperature.

4.4.2. Flowability results in Micro-part

Figure 4.18 and Figure 4.19 represents the results of numerical analysis of micro sized connector in accordance with flow rate. Figure 4.18 provides the numerical results obtained under slow flow rate of S1 and S2 respectively. As shown in Figure 4.18 due to slow flow rate both micro-connector of S1 and S2 could not filled the micro connector fully, also it was found that under slow flow rate, the species of material was not a significant factor. Therefore, regardless of the glass fiber length, volume fraction and thermal conductivity if the flow rate is not fast enough, it is difficult to fill the micro sized connector. A possible explanation for this might be that as a size of product is miniaturized, the shear rate and friction are significantly enhanced, thus, the material is solidified before filling the product. However, in Figure 4.19 with fast slow rate, it is apparent that numerical analysis showed that the connector was fully filled with S2, on the other hand, a short shot connector was obtained when S1 was used as material as represented Figure 4.19a this is because the glass fibers are clogged at the top part of micro connector which problem

can be verified in the Micro-CT images (this problem will talk later in detail).

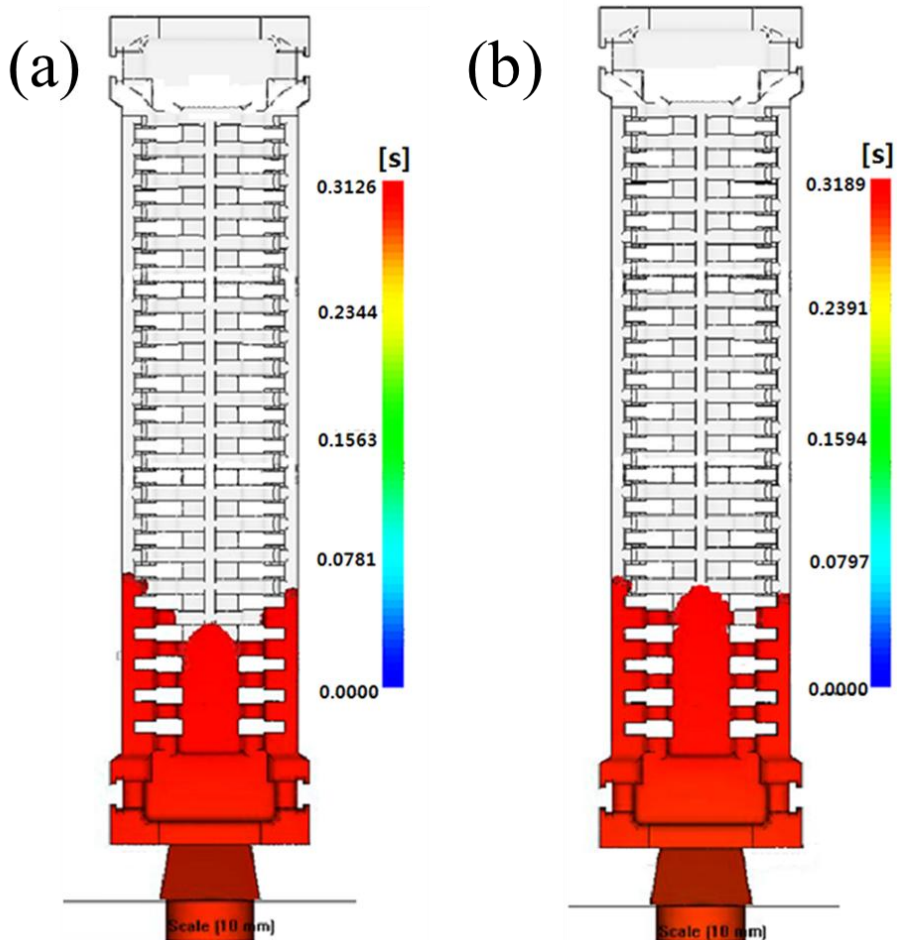


Figure 4.18. Numerical analysis results of (a) S1 and (b) S2 under slow flow rate.

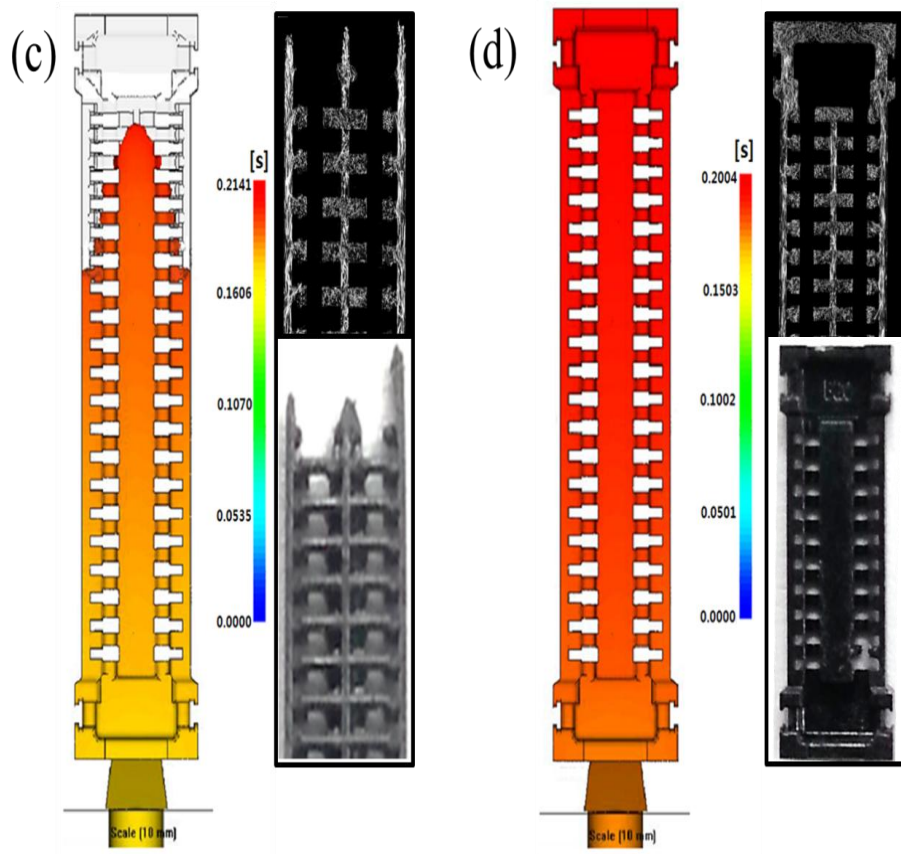


Figure 4.19. Numerical analysis results of (a) S1 and (b) S2 under fast flow rate with real images and Micro-CT images.

4.4.3. Result of Thermo Gravimetric Analysis (TGA)

We measured the residue of mass in local areas of the fully filled and short-shot parts in order to confirm the clogging by inclusions using TGA (Figure 4.20). The residue weight percent of half of the part near the short-shot gate part is 65.02 %. On the other hand, the residue weight percent of the opposite area is 67.09 %, which is higher than the residue weight percent of area near the gate. It is due to the fact that glass fibers were concentrated on the edge of melt-front area. Therefore, the molten composite could not go through further. However, it is shown that glass fibers for a completely filled part aligned well in flow paths, so that there was no glass fiber clogging. This tendency is also shown in the short-shot part on the side. The weight percent of half of the part near the gate is higher (67.09 %) than the opposite area (65.90 %), which elucidates the clogging due to glass fiber in a narrow width. These mass differences are not shown in completely filled part in which the residue weight percent of half of the part near the area is almost same as that of the opposite area. This means that the length and amount of glass fibers play a crucial role in fluidic properties of molten polymer composites

in a micro-molded part. These results will provide the understanding of the effect of inclusions and rheological properties of materials on the fluidic properties in micro-molded composite parts.

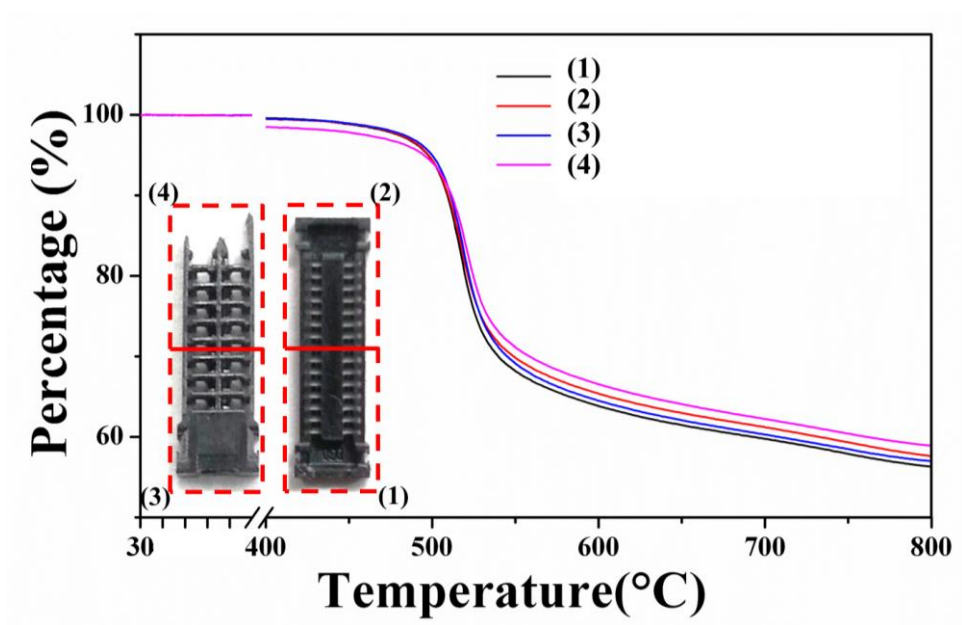


Figure 4.20. The ratio of mass differences as a function of temperature.

Table 3. Residue weight percent of each section at same temperature.

	Connector		Short shot connector	
	Gate section(1)	Opposite gate section(2)	Gate section (3)	Opposite gate section(4)
Residue (wt %)	64.37	65.90	65.02	67.09
Temperature (°C)	591.667	591.667	591.667	591.667

4.5. Thermal conductivity

4.5.1. Dependence of thermal conductivity coefficient

As it is mentioned above, thermal conductivity is one of the major variables to determine the viscosity owing to solidification rate. To establish the reliability of thermal conductivity, the numerical analysis was performed with different thermal conductivity coefficient. The results obtained from the numerical analysis of flowability with regard to different thermal conductivity coefficient can be compared in Figure 4.21, Figure 4.22 and Figure 4.23. As can be seen from the results, there was a significant difference according to thermal conductivity, i.e. solidification rate. As thermal conductivity value goes up, the flowability showed worse results. Particularly owing to higher thermal conductivity of S1, heat transfer between mold and melt occurs rapidly. Although melt has a high temperature at first (in this case 350 °C) melt temperature drops significantly as injection molding processed because of low temperature of mold (in this case 90 °C) which is the result of thermal equilibrium between melt and mold. As a result, solidified melt is clogged at the front of the stream

and blocks the flow of rest of the materials in the micro sized path. As shown in Figure 4.21, Figure 4.22 and Figure 4.23, from the comparison of the numerical analysis, it is found that as increase the thermal conductivity coefficient, the melt solidifies at closer the gate part.

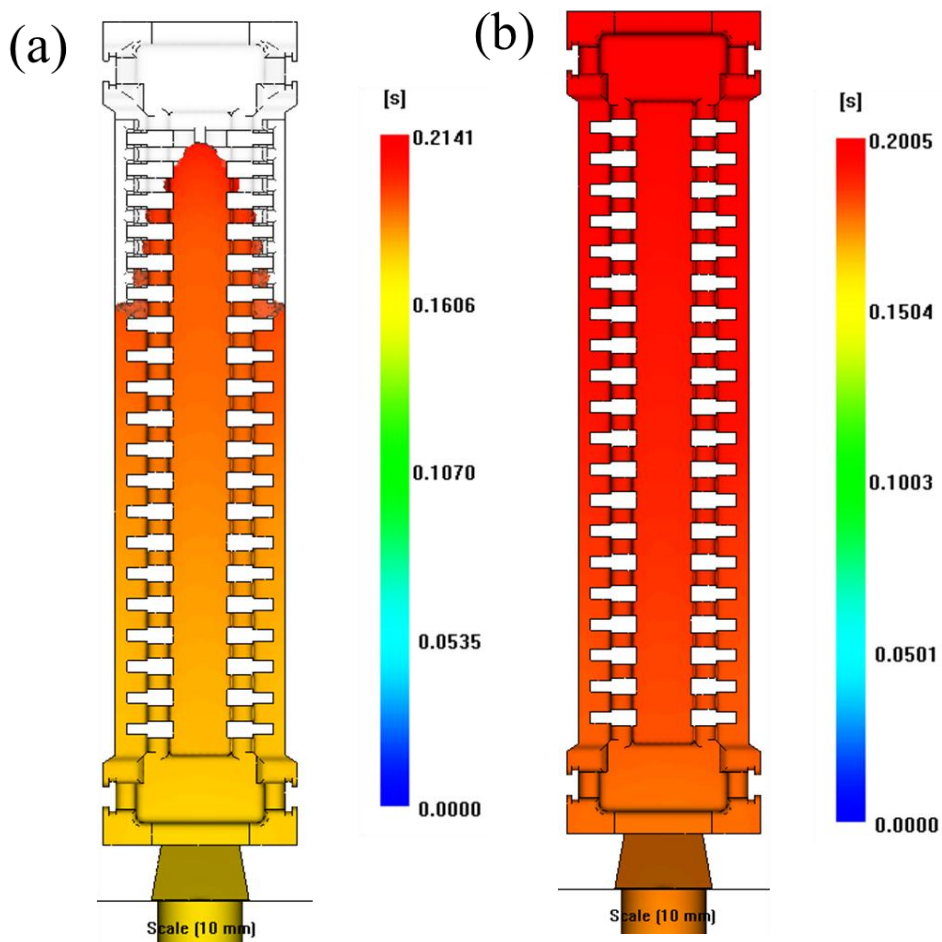


Figure 4.21. Numerical analysis results of (a) S1 and (b) S2 with same thermal conductivity coefficient ($0.9 \text{ W/m } ^\circ\text{C}$).

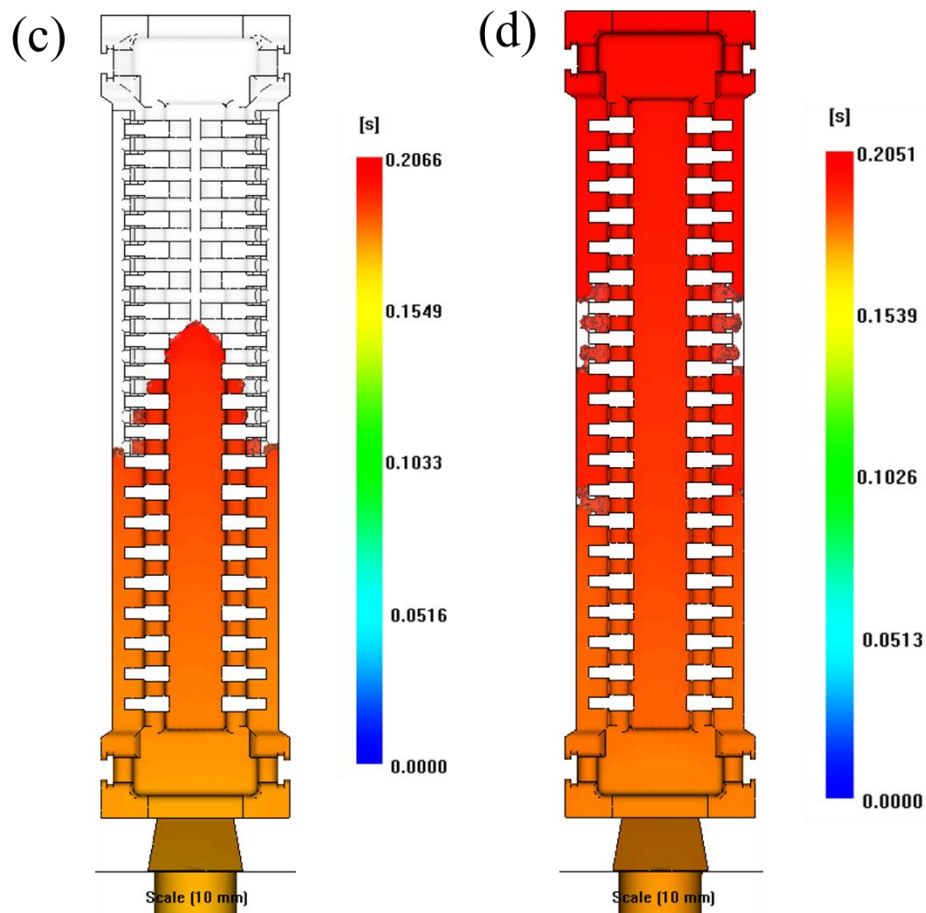


Figure 4.22. Numerical analysis results of (c) S1 and (d) S2 with same thermal conductivity coefficient (1.8 W/m °C).

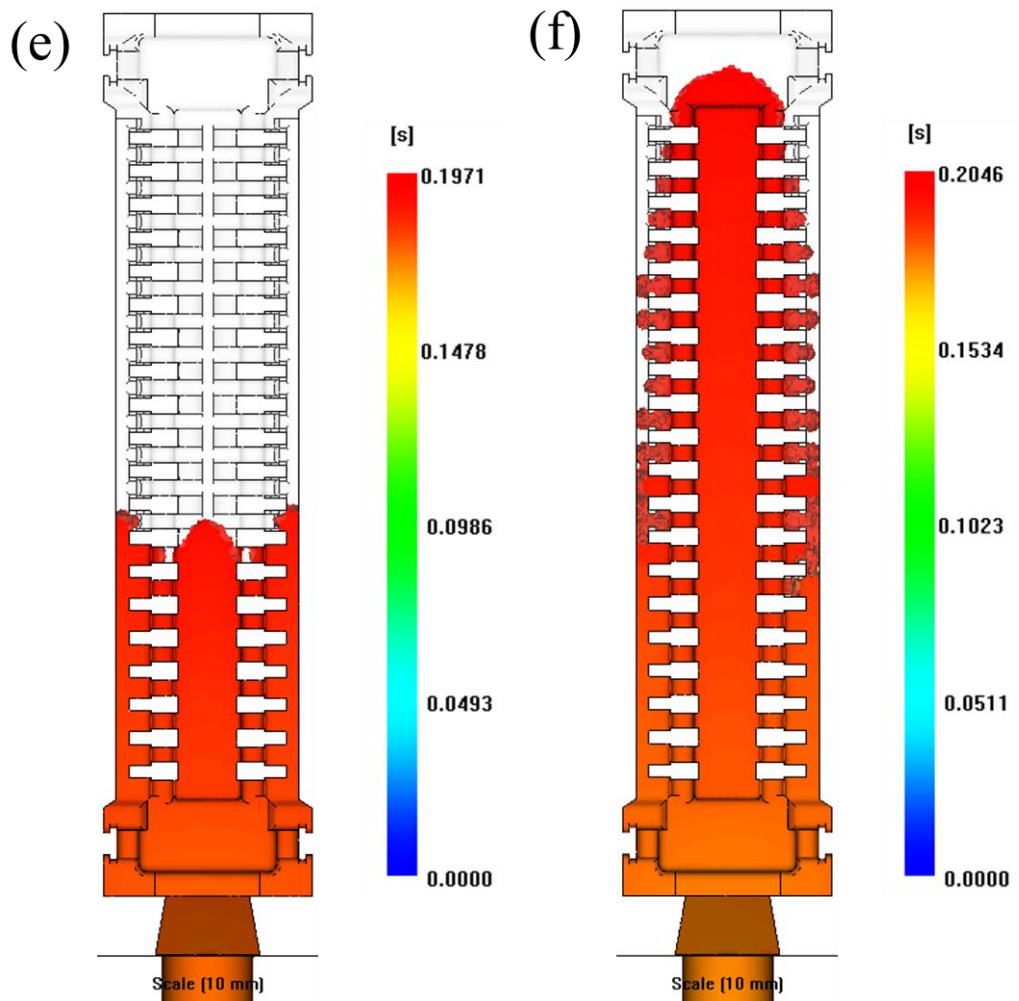
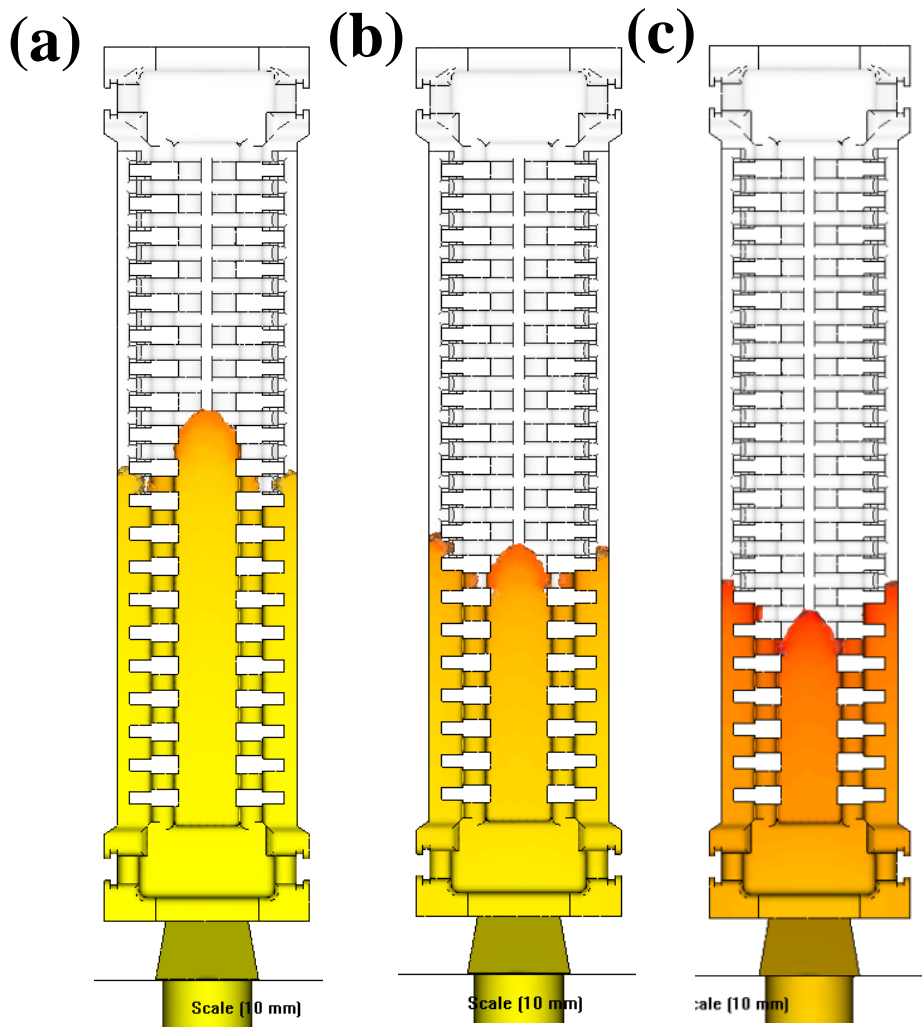


Figure 4.23. Numerical analysis results of (e) S1 and (f) S2 with same thermal conductivity coefficient ($2.5 \text{ W/m } ^\circ\text{C}$).

4.6. Cross WLF model and n coefficient

It is well known fact that generally a viscosity of fluid decreases with an increasing shear rate which is called shear thinning behavior. This behavior is found in molten polymers. We set the different values of coefficient of n from the Cross-WLF model to examine the flowability depends on different values of n , for example, when n is equal to 1 this means the Newtonian fluid. Figure 4.24 and Figure 4.25 compare the capability to fill the micro connector. It is verified that the result with lower value of n has a better capability to fill the micro connector. The reason for these behaviors is considered that complicated linked polymer chains come untangled under one axial high stress, hence, the polymers oriented the same direction with stress which leads to lower viscosity values.



**Figure 4.24. Numerical results of S1 with different value of n
 (a) 0.6 (b) 0.8 (c) 1.**

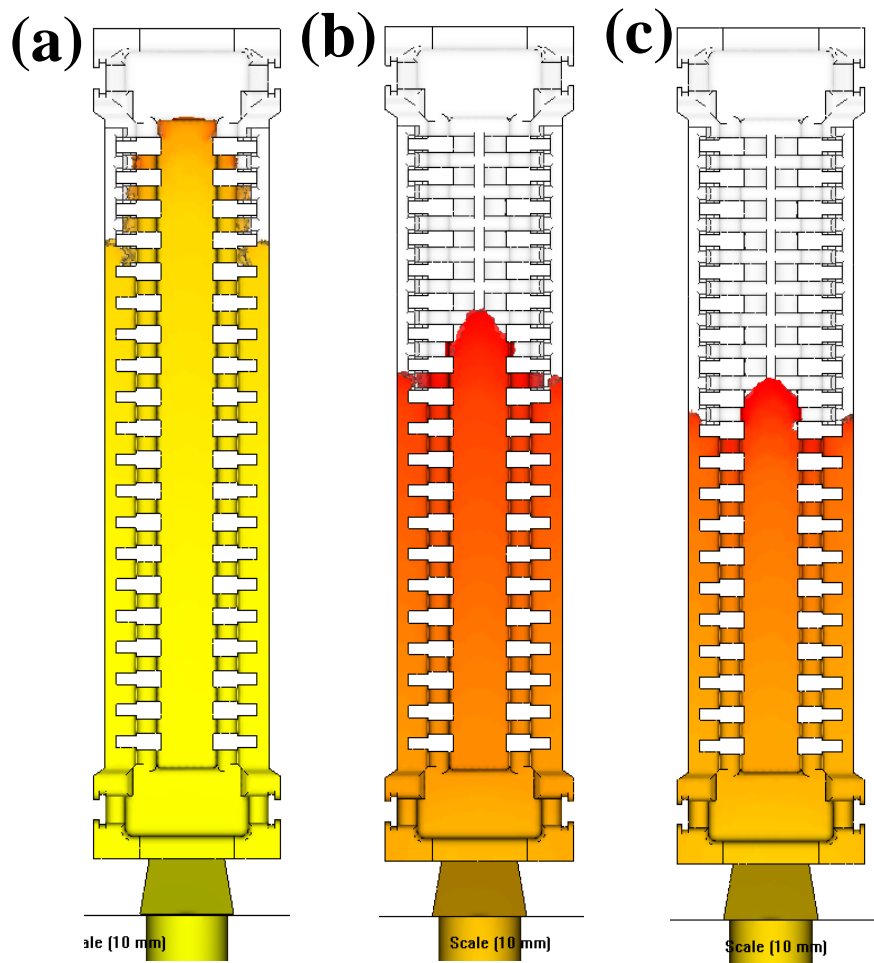


Figure 4.25. Numerical results of S2 with different value of n
(a) 0.6 (b) 0.8 (c) 1.

4.7. Real, Micro-CT, 3D images with line intensity analysis

It is worthy to note that, clogged glass fiber cause the short-shot micro connector during injection molding process within micro-sized narrow path since it acts as a hindrance. It becomes more obvious as the reinforcing fillers are observed in the micro-molded part by using Micro-CT. The micro-molded part in Figure 4.26 shows the fiber clogging at the front. The real image, Micro-CT image and the 3D structure indicate that the glass fibers are concentrated at the front section of micro connector (meaning, the picture shows more white colors at the front in the 2D Micro-CT image) which can be verified from the line spectrum in Fig 11.1. The intensity at the dashed blue line is translated as a function of distance quantitatively. It is apparent that the intensity at the clogged glass fiber area represent almost same intensity without fluctuation relatively, on the other hand, well oriented glass fiber area has a sever fluctuation compared with high density glass fiber area. The clogging result is confirmed clearly from the result of 3D volumetric image. This short-shot problem also occurs at the side channel through which the glass fibers were concentrated and clogged (Figure 4.27). Therefore, the flow does not

progress and is solidified before complete filling. On the other hand, it shows that glass fibers are distributed uniformly throughout the whole part for full filled one (Figure 4.28).

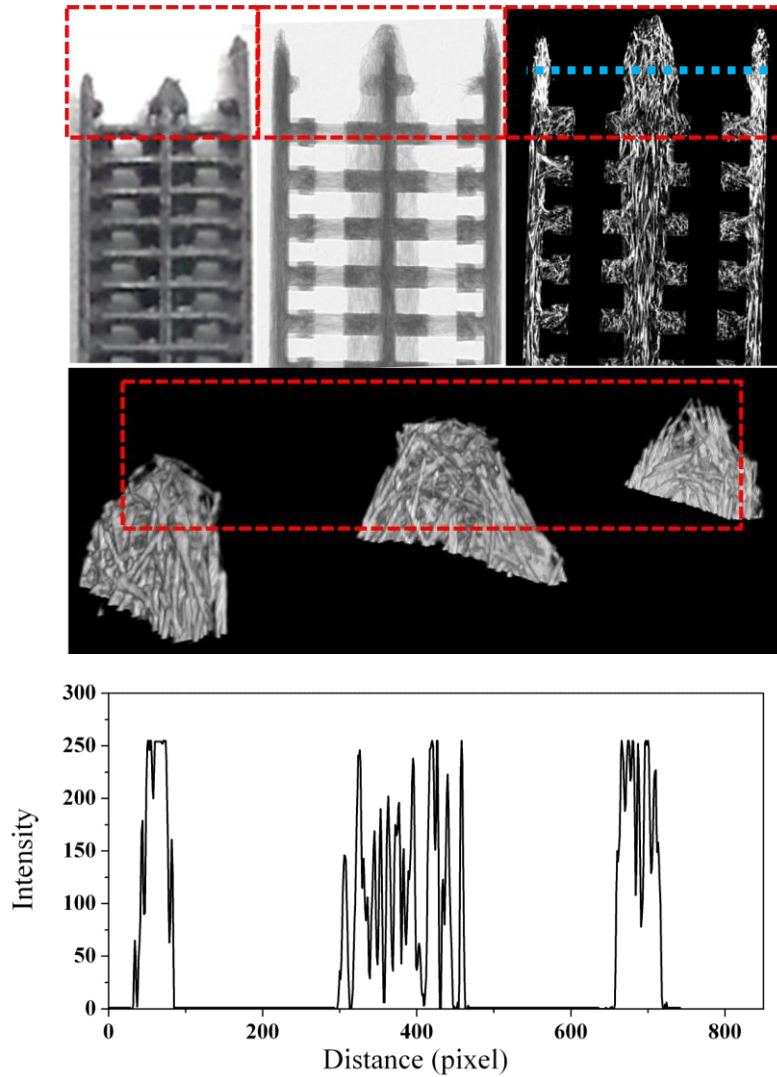


Figure 4.26. Images of Micro-CT , real micro connector and 3D construction of fiber clogging problem at the top part of micro connector and line spectrum of intensity.

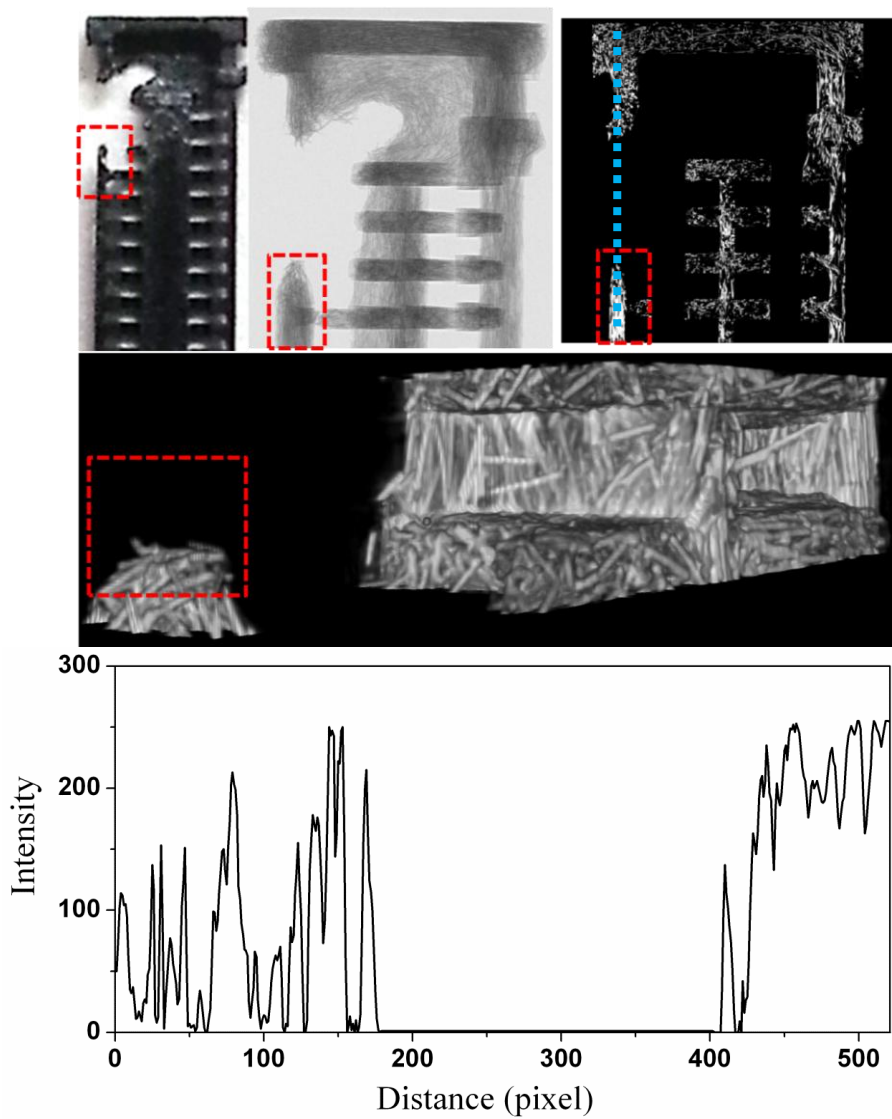


Figure 4.27. Images of Micro-CT , real micro connector and 3D construction of fiber clogging problem on the side part of micro connector and line spectrum of intensity.

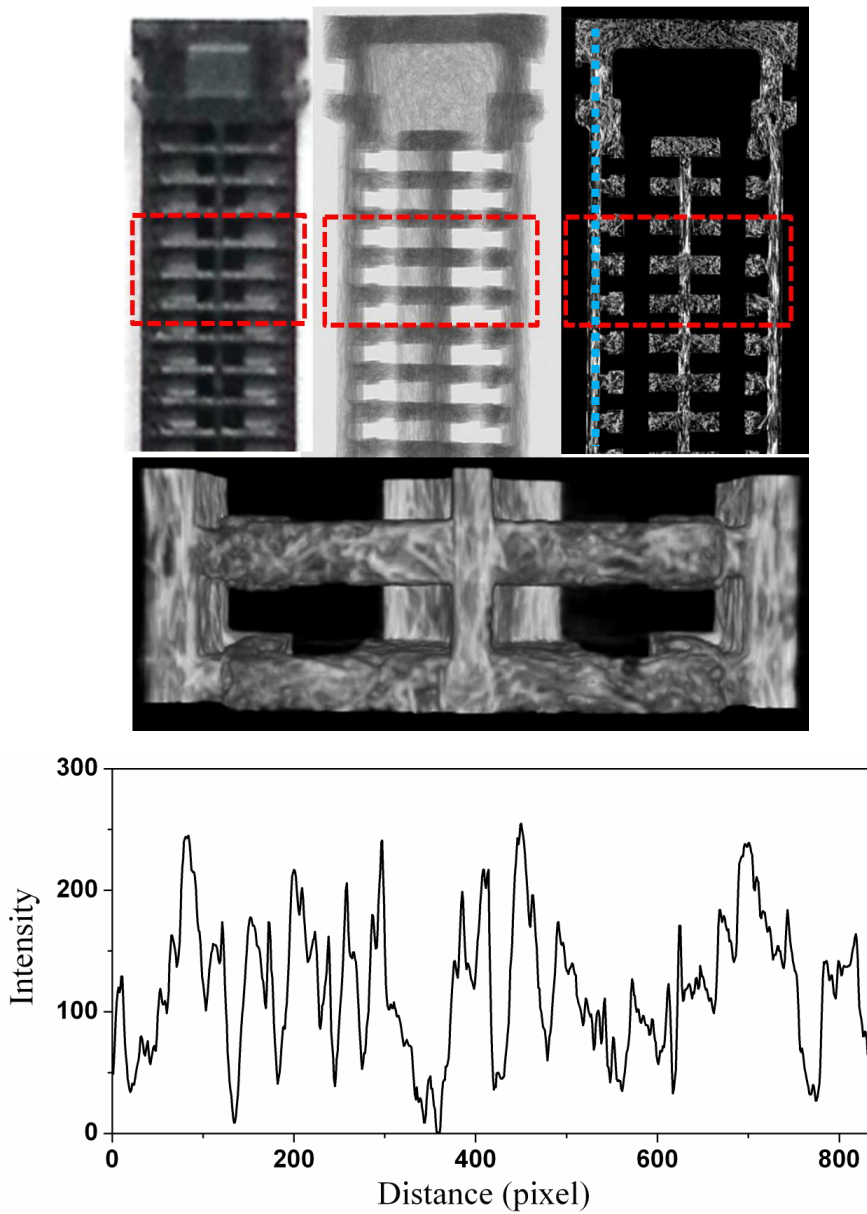


Figure 4.28. Images of Micro-CT , real micro connector and 3D construction for fully filled micro connector and line spectrum of intensity.

4.8. Effective elastic modulus

FLD is a useful method to evaluate the effective elastic modulus of polymer composites. It is applicable by combining theoretical models such as the Weibull, Log-normal and GEV statistical functions with FLD data obtained from an image processing. The effective elastic moduli of composite materials can be calculated by following equation according to Laminate Analogy Approach (LAA).

$$E_{ii} = \frac{A_{ii}A_{jj} - A_{ij}^2}{A_{jj}}$$

Where $A_{ij} = \int_{\text{Minimum Length}}^{\text{Maximum Length}} P_{ij}f(L)dL$, $f(L)$ indicates a probability distribution function obtained by FLD data, P_{ij} is the component of the stiffness matrix that relates the stress to the strain for the uniaxial ply. When i equals 1 i.e., E_{11} that indicates the longitudinal direction and when i equals 2 i.e., E_{22} , which presents the transverse direction of an elastic modulus. Since the difference of elastic moduli between talc and matrix is not significantly large, a small perturbed strain is expected. On the other hand, it is predicted large effective elastic modulus due to the perturbed strain caused by glass fibers. The

effective elastic moduli were presented as a function of volume fraction of glass fiber and total inclusion (Figure 4.29 and Figure 4.30). When the x value is zero, it means that the composite is completely filled with talc without glass fibers. As shown in Figure 4.29 the effective elastic moduli for S1 in regard to three statistical models indicate approximately 20 GPa, which are higher values than those of effective elastic moduli of S2 around 15 GPa. It is obvious that S2 shows more accurate values of theoretical effective elastic moduli compared with S1, moreover it has a good agreement with experimental data in the inset graph. It is considered that owing to longer length of glass fiber for S1 there was a greater perturbed strain than S2. As shown in Figure 4.30, the transverse direction of the effective elastic modulus was also characterized by using the Weibull, Log-normal and GEV theoretical models. However there was no significant difference between S1 and S2. The reason for this is shear resistance between glass fiber and matrix is not changed. As a result, the prediction of effective elastic modulus by using theoretical models is very effective approaching.

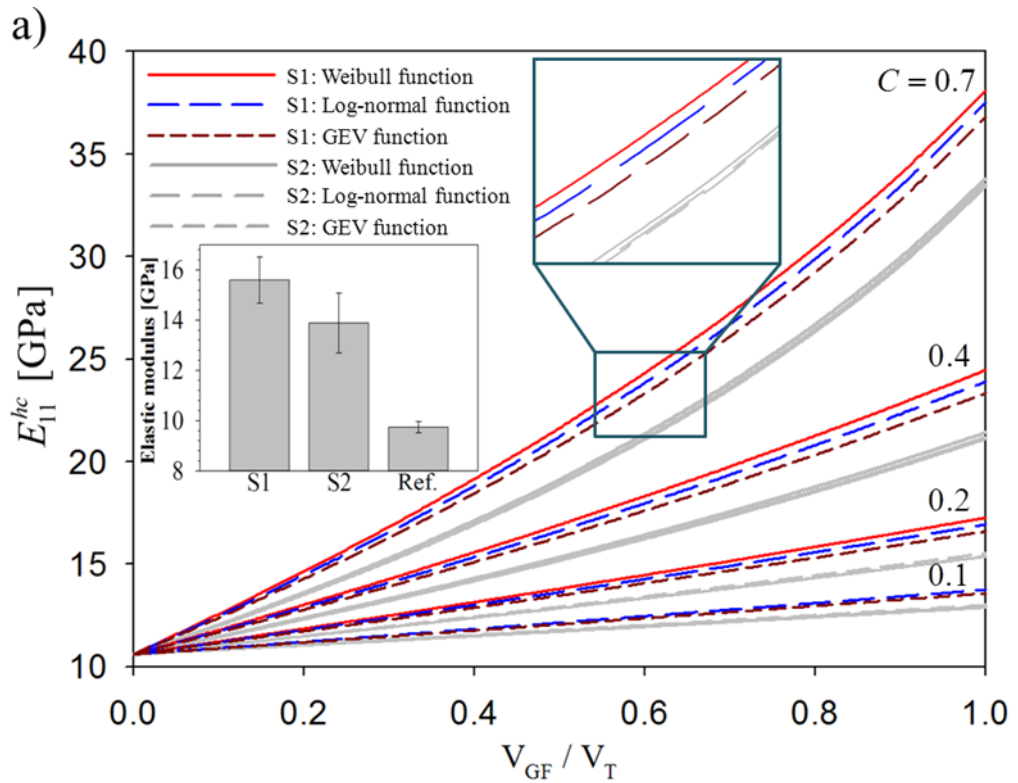


Figure 4.29. Longitudinal direction of effective elastic modulus as a function of ratio of glass fiber and total volume fraction with theoretical models for S1 and S2. The inset graph represents elastic modulus of S1, S2 and reference sample.

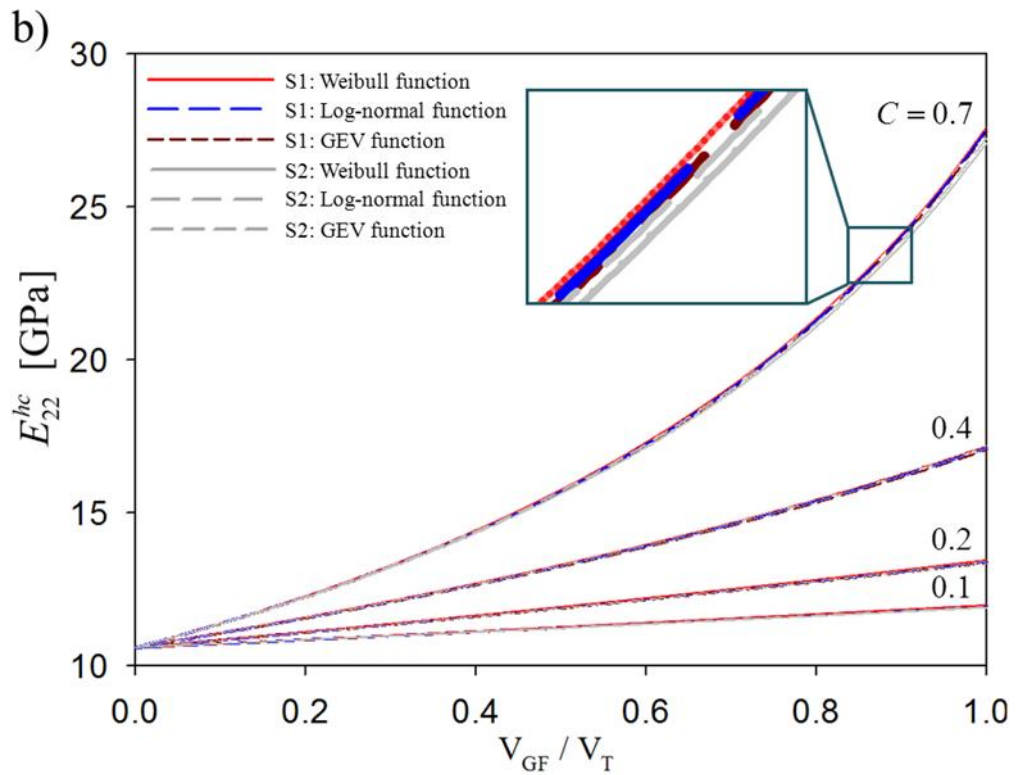


Figure 4.30. Transverse direction of effective elastic modulus as a function of ratio of glass fiber and total volume fraction with theoretical models for S1 and S2.

Figure 4.31 shows probability distribution functions with various log location parameters and log scale parameters to examine the effective elastic modulus by using the Log-normal theoretical model. Among the various probability distribution functions, the G5 with $\mu = 4.47$ and $\sigma = 0.79$ shows most accurate behavior compared with experimental data. Although G2 and G5 show similar behavior on probability distribution function, there was a great mismatch of the effective elastic modulus along the longitudinal direction as shown in Figure 4.32. This is suggested that, even though G2 and G5 are based on the same length of glass fibers, the prediction of the effective elastic modulus could be obtained inaccurately. Thus it is obvious that not only choosing the appropriate theoretical model but also choosing proper parameters are essential to predict accurate theoretical calculations. Also, Figure 4.33 indicates that there are no significant differences of the effective elastic moduli with various log location parameters and log scale parameters along the transverse direction, which means that the shear resistance between the glass fibers and matrix has not affected when the glass fibers are oriented along the longitudinal direction.

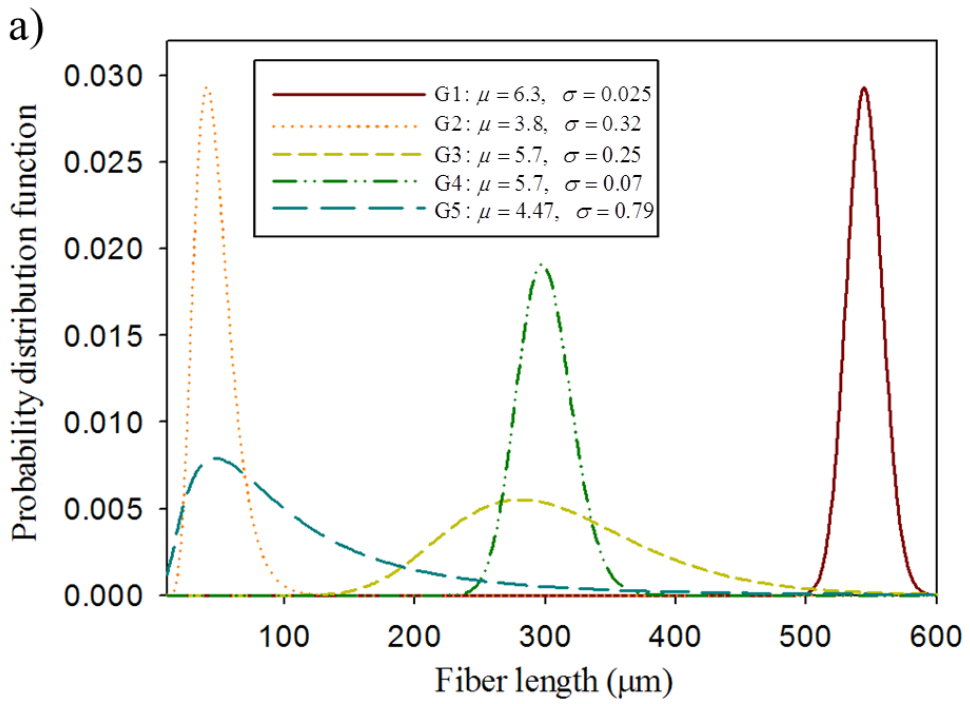


Figure 4.31. Probability distribution function with various log location parameters and log scale parameters.

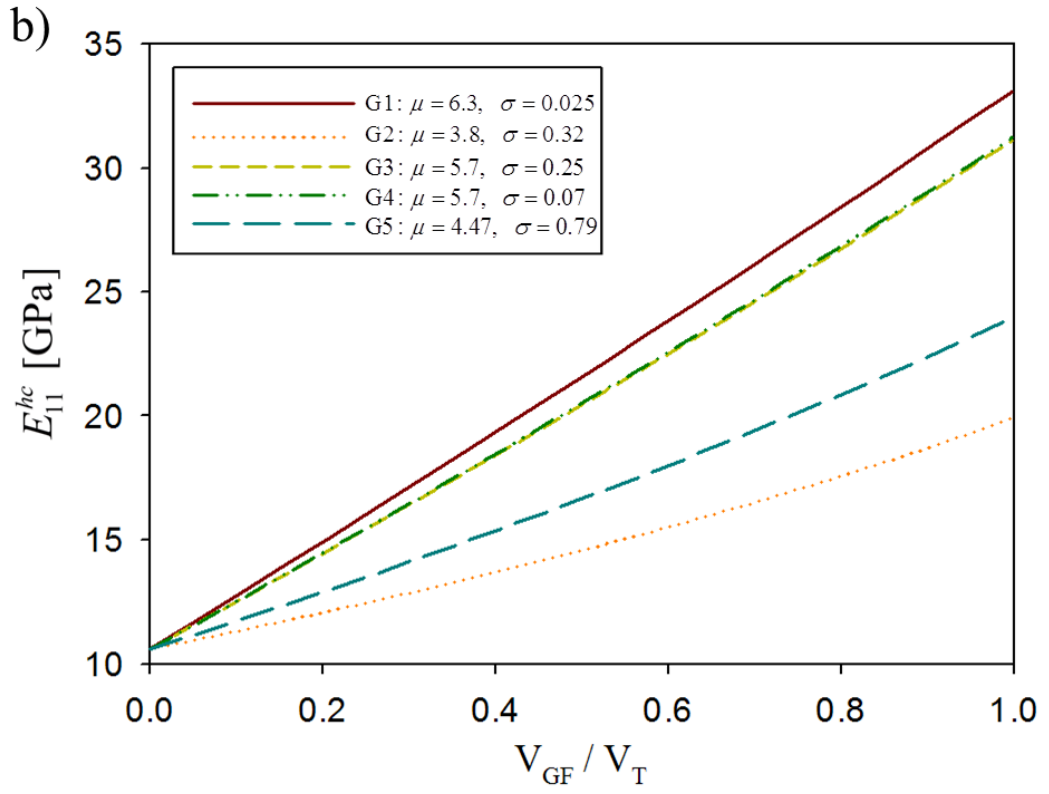


Figure 4.32. Theoretical effective elastic moduli along the longitudinal direction.

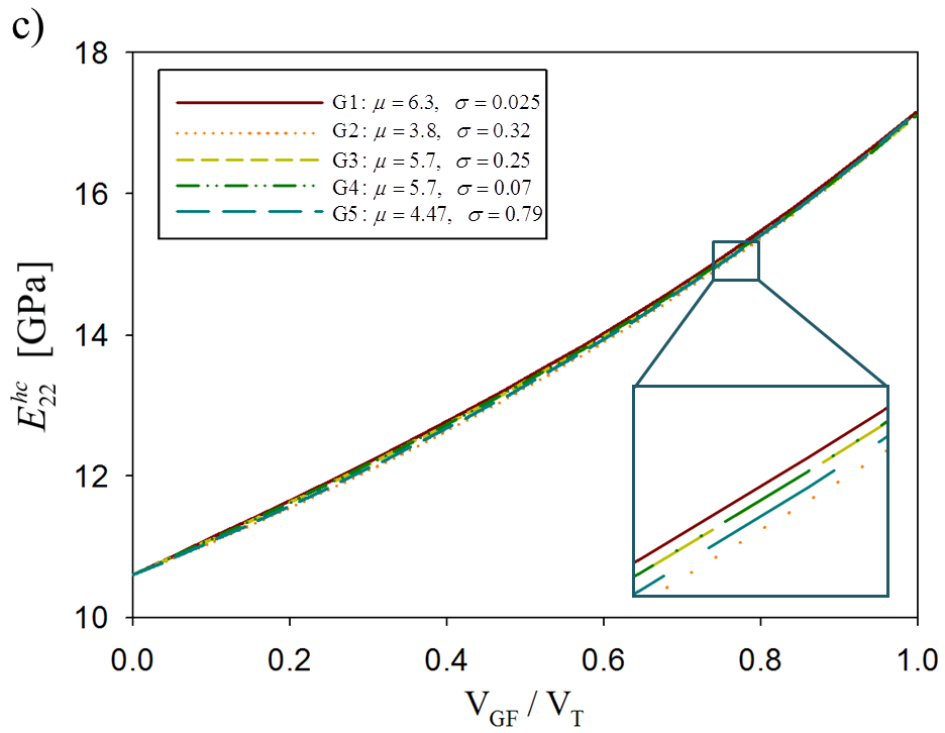


Figure 4.33. Theoretical effective elastic moduli along the transverse direction.

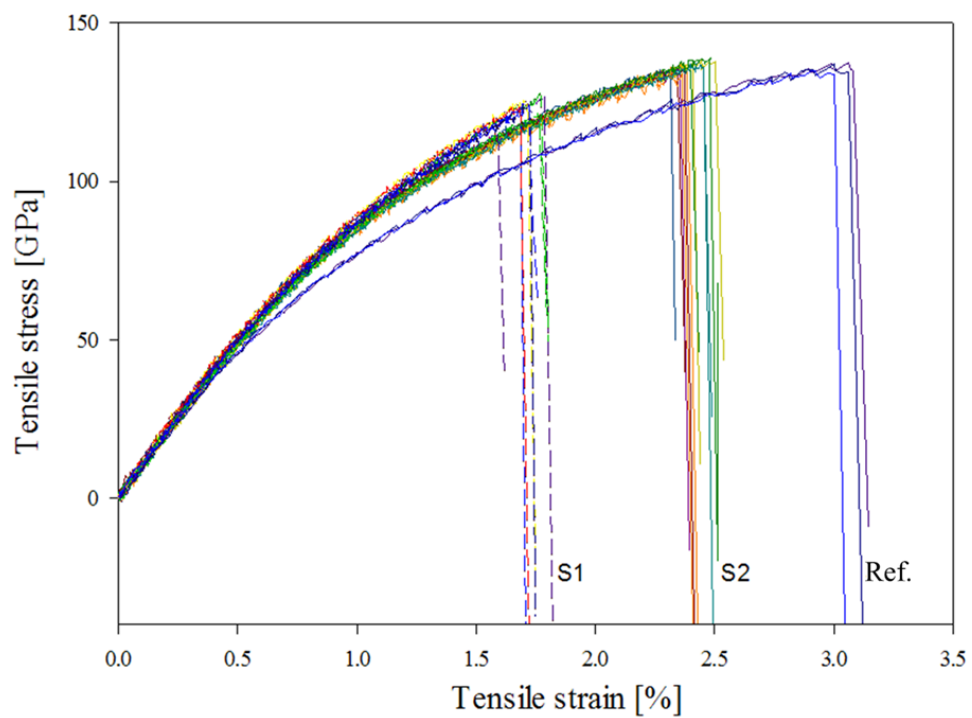


Figure 4.34. Tensile stress curves of S1, S2 and a reference sample with respect to tensile strain.

V. CONCLUSION

In this study, a flowability of composite materials was investigated by carrying out a numerical analysis to find out crucial parameters such as fiber length distribution, fiber volume fraction, and thermal conductivity of composite materials. The volume fraction of inclusions was obtained by an incineration method and the morphology of each specimen was obtained by SEM. The results of the coefficient of thermal expansion along the flow and transverse directions were measured by Thermo-mechanical analysis. A Micro-CT was used to observe the fiber length distribution inside the micromolded parts, and 3D internal structures were reconstructed by using the stacked images. The 3D images enabled us to determine and compare FLD quantitatively by converting the data into probability distribution functions, cumulative functions and distribution functions whose distributions are coincident with theoretical models, particularly the GEV distribution function. Based on the fiber length distribution results, it is indicated that long glass fibers inside the composite materials may attribute to low flowability, which indicates that fiber length and distribution are the main factor on the rheological

properties of the composite materials. It is worthy to note that fiber clogging inside the micro-sized pitches and channels was observed on the front tip and on the main channels of the micro connector due to the stereotactic hindrance of long length fibers. This problem was observed by Micro-CT results and quantitatively analyzed by TGA data. The statistical fiber breakage models confirmed that the length of glass fibers causes the difference of the flowability. Since thermal conductivity also plays an important role in heat transfer and energy dissipation of molten polymers which can cause the difference of the viscosities, it is necessary to verify the correlation between solidification rate and flowability. Therefore, a numerical analysis was performed to find out the correlation. The numerical analysis was employed by using the Cross-WLF viscosity model by changing the power-law index to investigate the effect of viscosity change on shear rate. The results show that high thermal conductivity has less flowability owing to an increased solidification rate. Consequently, it is found that flowability is significantly affected by the rheological properties of composite materials which closely relate to fiber volume fraction, fiber length distribution and thermal conductivity.

References

- [1] Sha B, Dimov S, Griffiths C, Packianather MS. Investigation of micro-injection moulding: Factors affecting the replication quality. *J Mater Process Tech.* 2007;183(2-3):284-296.
- [2] Wang YL, Yue CY, Tam KC, Hue X. Relationship between processing, microstructure, and mechanical properties of injection molded thermotropic LCP. *J Appl Polym Sci.* 2003;88(7):1713-1718.
- [3] Garcia M, Eguiazabal JI, Nazabal J. Two scale reinforcement in hybrid composites based on poly(ether sulfone), glass fiber and liquid crystalline polymer. *Compos Sci Technol.* 2003;63(15):2163-2170.
- [4] Tjong SC. Structure, morphology, mechanical and thermal characteristics of the in situ composites based on liquid crystalline polymers and thermoplastics. *Mat Sci Eng R.* 2003;41(1-2):1-60.
- [5] Arbelaiz A, Fernandez B, Cantero G, Llano-Ponte R, Valea A, Mondragon I. Mechanical properties of flax fibre/polypropylene composites. Influence of fibre/matrix modification and glass fibre hybridization. *Compos Part a-Appl S.* 2005;36(12):1637-1644.
- [6] Shen HB, Nutt S, Hull D. Direct observation and measurement of fiber architecture in short fiber-polymer composite foam through micro-CT imaging. *Compos Sci Technol.* 2004;64(13-14):2113-2120.

- [7] Wu SH, Wang FY, Ma CCM, Chang WC, Kuo CT, Kuan HC, et al. Mechanical, thermal and morphological properties of glass fiber and carbon fiber reinforced polyamide-6 and polyamide-6/clay nanocomposites. *Mater Lett.* 2001;49(6):327-333.
- [8] Clarke AR, Archenhold G, Davidson NC. A Novel Technique for Determining the 3d Spatial-Distribution of Glass-Fibers in Polymer Composites. *Compos Sci Technol.* 1995;55(1):75-91.
- [9] Eberhardt C, Clarke A. Fibre-orientation measurements in short-glass-fibre composites. Part I: automated, high-angular-resolution measurement by confocal microscopy. *Compos Sci Technol.* 2001;61(10):1389-1400.
- [10] O'Connell MK, Murthy S, Phan S, Xu C, Buchanan J, Spilker R, et al. The three-dimensional micro- and nanostructure of the aortic medial lamellar unit measured using 3D confocal and electron microscopy imaging. *Matrix Biol.* 2008;27(3):171-181.
- [11] Roux S, Hild F, Viot P, Bernard D. Three-dimensional image correlation from X-ray computed tomography of solid foam. *Compos Part a-Appl S.* 2008;39(8):1253-1265.
- [12] Schilling PJ, Karedla BPR, Tatiparthi AK, Verges MA, Herrington PD. X-ray computed microtomography of internal damage in fiber reinforced polymer matrix composites. *Compos Sci Technol.* 2005;65(14):2071-2078.
- [13] Chiang YC, Hickel R, Lin CP, Kunzelmann KH. Shrinkage vector

- determination of dental composite by μ CT images. *Compos Sci Technol.* 2010;70(6):989-994.
- [14] Lee DJ, Oh H, Song YS, Youn JR. Analysis of effective elastic modulus for multiphased hybrid composites. *Compos Sci Technol.* 2012;72(2):278-283.
- [15] Awaja F, Nguyen MT, Zhang SN, Arhatari B. The investigation of inner structural damage of UV and heat degraded polymer composites using X-ray micro CT. *Compos Part a-Appl S.* 2011;42(4):408-418.
- [16] Renghini C, Komlev V, Fiori F, Verne E, Baino F, Vitale-Brovarone C. Micro-CT studies on 3-D bioactive glass-ceramic scaffolds for bone regeneration. *Acta Biomater.* 2009;5(4):1328-1337.
- [17] Jiang YB, Zhao J, Liao EY, Dai RC, Wu XP, Genant HK. Application of micro-CT assessment of 3-D bone microstructure in preclinical and clinical studies. *J Bone Miner Metab.* 2005;23:122-131.
- [18] Fu SY, Lauke B. Effects of fiber length and fiber orientation distributions on the tensile strength of short-fiber-reinforced polymers. *Compos Sci Technol.* 1996;56(10):1179-1190.
- [19] Hine PJ, Lusti HR, Gusev AA. Numerical simulation of the effects of volume fraction, aspect ratio and fibre length distribution on the elastic and thermoelastic properties of short fibre composites. *Compos Sci Technol.* 2002;62(10-11):1445-1453.

- [20] Thomason JL, Vlugg MA. Influence of fibre length and concentration on the properties of glass fibre-reinforced polypropylene .1. Tensile and flexural modulus. *Compos Part a-Appl S.* 1996;27(6):477-484.
- [21] Weber M, Kamal MR. Estimation of the volume resistivity of electrically conductive composites. *Polym Composite.* 1997;18(6):711-725.
- [22] Agari Y, Ueda A, Nagai S. Thermal-Conductivity of a Polyethylene Filled with Disoriented Short-Cut Carbon-Fibers. *J Appl Polym Sci.* 1991;43(6):1117-1124.
- [23] Fu SY, Mai YW. Thermal conductivity of misaligned short-fiber-reinforced polymer composites. *J Appl Polym Sci.* 2003;88(6):1497-1505.
- [24] Thomason JL, Groenewoud WM. The influence of fibre length and concentration on the properties of glass fibre reinforced polypropylene .2. Thermal properties. *Compos Part a-Appl S.* 1996;27(7):555-565.
- [25] Crowson RJ, Folkes MJ. Rheology of Short Glass Fiber-Reinforced Thermoplastics and Its Application to Injection-Molding .2. The Effect of Material Parameters. *Polym Eng Sci.* 1980;20(14):934-940.
- [26] Pipes RB, Hearle JWS, Beaussart AJ, Okine RK. Influence of Fiber Length on the Viscous-Flow of an Oriented Fiber Assembly. *J Compos Mater.* 1991;25(10):1379-1390.
- [27] Carneiro OS, Maia JM. Rheological behavior of (short) carbon fiber/thermoplastic composites. Part II: The influence of matrix type. *Polym*

Composite. 2000;21(6):970-977.

[28] Potschke P, Fornes TD, Paul DR. Rheological behavior of multiwalled carbon nanotube/polycarbonate composites. *Polymer*. 2002;43(11):3247-3255.

[29] Silva ALN, Rocha MCG, Coutinho FMB. Study of rheological behavior of elastomer/polypropylene blends. *Polym Test*. 2002;21(3):289-293.

[30] Murshed SMS, Leong KC, Yang C. Investigations of thermal conductivity and viscosity of nanofluids. *Int J Therm Sci*. 2008;47(5):560-568.

[31] Thomasset J, Carreau PJ, Sanschagrin B, Ausias G. Rheological properties of long glass fiber filled polypropylene. *J Non-Newton Fluid*. 2005;125(1):25-34.

[32] Seeton CJ. Viscosity-temperature correlation for liquids. *Tribol Lett*. 2006;22(1):67-78.

[33] Vanvelze.D, Cardozo RL, Langenka.H. Liquid Viscosity-Temperature-Chemical Constitution Relation for Organic Compounds. *Ind Eng Chem Fund*. 1972;11(1):20-&.

초 록

사출 공정은 자동차의 범퍼, 텔레비전의 베젤 등과 같은 대형제품과 복잡한 모양의 제품을 대량 생산할 수 있는 장점을 가지고 있다. 하지만 제품의 크기가 마이크로 사이즈로 소형화됨에 따라 사출 공정에서의 재료에 따른 흐름성이 중요해지고 있는 추세이다. 본 연구에서는 유리 섬유가 포함된 재료를 이용하여 부피 분율, 유리 섬유의 길이 분포와 열전도도가 흐름성에 어떠한 영향을 주는지 분석하였다. 복합재료에 포함된 유리 섬유와 미네랄의 부피 분율을 알아보기 위하여 회분 분석을 실시하였고, 회분 분석으로 얻어진 시편을 이용하여 SEM 촬영을 통하여 복합재료에 포함된 유리 섬유의 길이 차이를 확인하였다. 섬유의 길이 분포 측정을 위하여 마이크로-컴퓨터단층촬영을 실시하였으며, 얻어진 이미지를 이용하여 정량적으로 길이에 따른 섬유의 분포를 확인하였고 이미지를 적층하여 3D 구조로 구현하여 유리 섬유의 길이 차이와 분포를 확인하였다. 또한 열전도도에 따른 흐름성을 상용 프로그램 MOLDFLOW를 이용하여 분석하였다. 스파이럴 형태의 금형을 이용한 사출 공정 실험의 흐름성 결과와 수치해석적 해석이 일치함을 확인하였으며 완전하게 충전이 되지 않은 마이크로 커넥터의 마이크로-컴퓨터단층촬영을 통하여

마이크로 커넥터 내부의 섬유 물림 현상을 확인하여 원인을 분석하였으며 MOLDFLOW를 이용하여 얻어진 수치해석 결과와 일치함을 확인하였다.

주요어 : 마이크로 사출 성형, 섬유 길이 분포, 3D 구조, 복합재료 ,
수치해석

학번 : 2012-20643